AD-A079 113 STANFORD UNIV CALIF INTEGRATED CIRCUITS LAB F/G 17/1
FABRICATION, CHARACTERIZATION AND OPTIMIZATION OF POSFET (PVF2---ETC(U)
OCT 79 J D PLUMMER N00014-78-C-0614
UNCLASSIFIED TR-FR-DPG582 NL

1 OF 1
AD
A079113

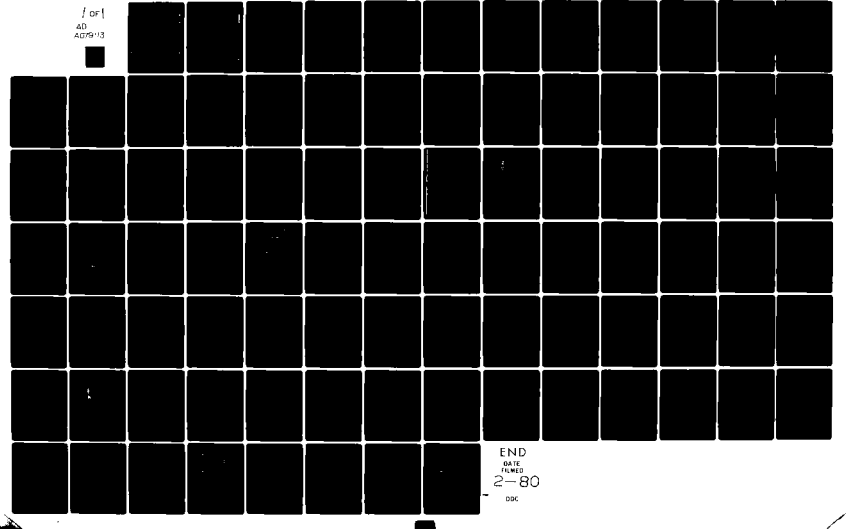

END
DATE FILMED
2-80
DDC

SECURITY CLASSIFICATION OF THIS PAGE *(When Data Entered)*

REPORT DOCUMENTATION PAGE

READ INSTRUCTIONS BEFORE COMPLETING FORM

1. REPORT NUMBER: TR-FR-DPG582
2. GOVT ACCESSION NO.
3. RECIPIENT'S CATALOG NUMBER

4. TITLE *(and Subtitle)*: Fabrication, Characterization and Optimization of Posfet (PVF_2-Silicon) Piezoelectric Transducers for Low Frequency (100 H_z to 500 kH_z) Underwater Acoustic Applications

5. TYPE OF REPORT & PERIOD COVERED: Final Report 1 Jul [illegible]78-31Aug[illegible]1979

6. PERFORMING ORG. REPORT NUMBER

7. AUTHOR(s): James D. Plummer, Ph.D.

8. CONTRACT OR GRANT NUMBER(s): N00014-78-C-0614

9. PERFORMING ORGANIZATION NAME AND ADDRESS: Stanford University, Integrated Circuits Laboratory, Stanford, CA 94305

10. PROGRAM ELEMENT, PROJECT, TASK AREA & WORK UNIT NUMBERS

11. CONTROLLING OFFICE NAME AND ADDRESS: Underwater Sound Reference Division, Naval Research Laboratory, P.O. Box 8337, Orlando, Florida 32806

12. REPORT DATE: Oct[illegible]979

13. NUMBER OF PAGES

14. MONITORING AGENCY NAME & ADDRESS(if different from Controlling Office)

LEVEL II

15. SECURITY CLASS. *(of this report)*: Unclassified

15a. DECLASSIFICATION/DOWNGRADING SCHEDULE

16. DISTRIBUTION STATEMENT *(of this Report)*: Unlimited

17. DISTRIBUTION STATEMENT *(of the abstract entered in Block 20, if different from Report)*

18. SUPPLEMENTARY NOTES: This contract is awarded under basic agreement N00014-78-C-0614 and modifications P00001 and P00002 dated 1 July 1978 issued by the Office of Naval Research, Department of Navy

19. KEY WORDS *(Continue on reverse side if necessary and identify by block number)*: Acoustic Transducers, Hydrophones, PVF_2, Silicon/PVF_2 Integrated Arrays

20. ABSTRACT *(Continue on reverse side if necessary and identify by block number)*

PVF_2 is a new organic polymer piezoelectric material. It's unique features include an acoustic impedance closely matched to liquid environments, linearity to a broad range of input signals, wide bandwidth and mechanical strength and flexibility. In comparison with commonly used ceramic piezoelectric materials, PVF_2 has a lower electromechanical coupling coefficient ~~(0.2 vs.~~ 0.49 ~~for PZT-5A)~~, a lower dielectric constant (11.5 ε_0 vs. 830 ε_0 ~~for PZT-5A~~) and higher dielectric losses at frequencies >500 KH_z. Because

DD FORM 1 JAN 73 1473 EDITION OF 1 NOV 65 IS OBSOLETE

Unclassified

SECURITY CLASSIFICATION OF THIS PAGE *(When Data Entered)*

GREATER THAN [illegible]

of these different material properties system applications of PVF_2 require different trade-offs than the ceramic materials. This report describes an investigation, both theoretical and experimental, of the potential applications of PVF_2 in low frequency (100 H_z-500 KH_z) underwater sound applications. Both reception and transmission of sound are considered and the experimental performance of several types of PVF_2 and integrated silicon/PVF_2 transducers are described.

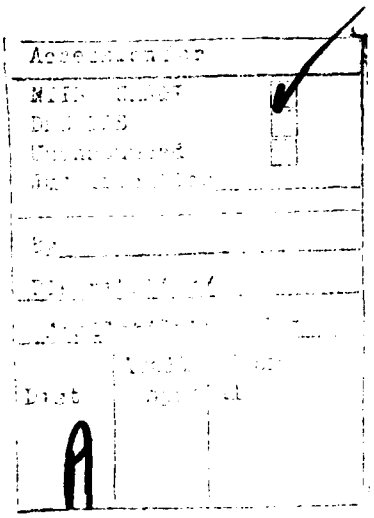

FABRICATION, CHARACTERIZATION AND OPTIMIZATION OF POSFET (PVF_2-SILICON) PIEZOELECTRIC TRANSDUCERS FOR LOW FREQUENCY (100 Hz to 500 kHz) UNDERWATER ACOUSTIC APPLICATIONS

Final Technical Report

Contract No. N00014-78-C-0614
Naval Research Laboratory
Underwater Sound Reference Division
P.O. Box 8337, Orlando, Florida 32806

by

James D. Plummer
Associate Professor
Electrical Engineering Department

Fabrication, Characterization and Optimization of Posfet (PVF_2-Silicon) Piezoelectric Transducers for Low Frequency (100 Hz to 500 kHz) Underwater Acoustic Applications

INTRODUCTION

Most underwater sound transducers used today contain polarized ferroelectric ceramics as the acoustic transduction elements. Applications include hydrophones, shock sensors and underwater projectors (transmitters of acoustic energy). The advantages of these ceramics include good piezoelectric coupling coefficients and high dielectric constants; however, these advantages are offset to some extent by high density, fragility, cost and limited sizes. Therefore, other materials should be investigated for possible applications. Piezoelectric polymers, such as PVF_2, are examples of such materials.

Recent work in the Integrated Circuits Laboratory and previously in the E.L. Gintzon Laboratory [1] at Stanford, has demonstrated both theoretically and experimentally, the substantial promise of PVF_2 for high frequency medical imaging and non-destructive testing systems in the 1-20 MHz frequency range. The recent development in the Integrated Circuits Laboratory of an integrated PVF_2-Si transducer structure (the Posfet), has clearly demonstrated the possibility of batch fabrication of high performance single elements and arrays of piezoelectric transducers. A vigorous program to apply this technology and these arrays to medical imaging in the 1-10 MHz range has been underway for some time in the Stanford Integrated Circuits Laboratory, under the support of the National Institutes of Health.

Application of PVF_2 transducers to lower frequency underwater applications requires additional basic information on the material's piezo-

electric behavior at low frequencies and high pressures and on the suitability of various mounting and backing materials and structures. It was the expressed purpose of this contract to investigate some of these questions both theoretically and experimentally and to fabricate a small number of prototype PVF_2 transducers suitable for characterization at low frequencies.

This report is organized as follows:

1. Introduction to PVF_2 and Posfet Transducer Structures and Arrays
2. Analyses and Modeling of the Posfet Transducer
3. Low frequency Considerations in PVF_2 and Posfet Transducers
4. Experimental Results on PVF_2 Transducers and Posfet Arrays as Receivers
5. Considerations Relating to the Use of PVF_2 as a Transmitter
6. Summary and Conclusions

I. Introduction to PVF_2 and Posfet Transducer Structures and Arrays

PVF_2 is an organic polymer material in which piezoelectric properties have recently been discovered [2.3]. Piezoelectricity can be induced in this material by stretching a film of the material to several times its original length. The stretching is done at elevated temperatures (typically 100-150°C). A static electric field (about 300 kV/cm) is applied perpendicular to the stretched direction (i.e., across the thickness of the film). Following the stretching operation, the film is slowly cooled back to room temperature with the electric field applied. At the completion of this poling process, electrodes can be applied to one or both sides of the transducer. If the poling process is properly done, the piezoelectric effects in the material are stable for long periods of time [3]. The origin of the piezoelectricity is not yet fully understood, although it is thought that the poling process increases true and/or polarization charges in the film through three kinds of processes - injection of homocharge from the electrode, dipole orientation in the film, and true charge separation in the film [1].

Experimental transducers were made with these films about four years ago in the Stanford E.K. Ginzton Laboratory [4]. Typically the transducers were constructed as shown in Fig. 1. The PVF_2 material was simply mounted with epoxy on a brass backing which serves as an acoustic backing and provides mechanical support. Transducer thicknesses of both 25 microns and 50 microns were evaluated.

The lateral dimensions of the PVF_2 films in these experiments were large compared to the thickness so that the transducers vibrate in the thickness mode. Since the brass backing has a high acoustic impedance relative to PVF_2 (approximately 10 times higher) the resonant frequency of the transducer is close to the quarter-wave frequency, rather than the more commonly encountered half-wave frequency with ceramic piezoelectrics. The thickness resonant fre-

quencies of the two transducers were, therefore, approximately 20 MHz and 10 MHz for the 25 micron and 50 micron films respectively.

The key results of these experimental measurements were the following [4].

1. The frequency response of the PVF_2 transducers was essentially flat from 0 to 25 MHz in the case of the 25 micron transducer and flat from 0 to 10 MHz in the 50 micron sample. (It should be pointed out, however, in the context of this resport, that detailed measurements of the acoustic response in the frequency range below 100kHz were apparently not made in these early experiments.)

2. The receiving sensitivity of each of the transducers was of the same magnitude as commerically available broadband PZT transducers.

3. Since the acoustic impedance of PVF_2 is close to that of water (4×10^6 vs. 1.5×10^6 kg/m2 sec), no matching layer was required on the front of the transducer to achieve these results.

Because of the low acoustic impedance of PVF_2 films, it is possible to use silicon (acoustic impedance approximately 19.7×10^6) as a "rigid" backing for the PVF_2. Thus we can achieve the same type of $\lambda/4$ resonant structure as was described above with a brass backing, using silicon. The direct analogy with this type of operation using ceramic transducers is not possible with a silicon backing because of the much higher acoustic impedances of typical piezoelectric ceramics. PzT has an acoustic impedance of 35×10^6 kg/m^2 sec and lead metaniobate about 20×10^6 kg/m^2 sec).

If we use silicon as a backing material for the PVF_2 transducer as shown in Fig. 2, the entire advanced capability of silicon technology and silicon devices becomes available as an integral part of the transducer structure. This new capability is distinct from two-dimensional pizoelectric arrays previously fabricated in the Integrated Circuits Laboratry at Stanford [5] since these earlier arrays used completely separate transducer cells and silicon devices which were interconnected after each was complete.

The lower electrode is shown in Fig. 2 as part of the silicon structure. This will become clearer later when devices are added to the silicon. To assemble the structure therefore, PVF_2 with metallization on only the top side would be attached with a nonconductive epoxy to a silicon wafer which already contains the lower electrode. Nonuniformities in the epoxy thickness

are of little consequence as explained below, but care must be taken to insure that no air gaps or bubbles are allowed between the two layers and to minimize the thickness of the epoxy layer.

As an example, for a resonant frequency of 3 MHz, the PVF_2 film would be approximately 175 microns thick. Since the maximum thickness of SiO_2 or other insulators which might be present on the silicon due to the presence of transistors, etc. would be $\sim$1 micron, these insulating layers should have virtually no effect on the acoustic performance of the structure. Similarly, the presence of epoxy to physically attach the PVF_2 to the silicon should have very little acoustic effect since the epoxy thickness would be expected to be just a few microns [6]. Both the SiO_2 and epoxy have dielectric constants roughly the same as PVF_2 (approximately 5-13 depending on frequency) and thus they appear electrically as capacitors in series with the PVF_2 but much larger (10 to 100 times) and hence of little importance. (The one exception to this statement, will be described later in this section.)

The top face of the transducer requires no matching into water because of the relatively low impedance of PVF_2. A thin waterproofing layer may be added to the top face if necessary. On the backside of the silicon an appropriate acoustically matched layer is added which may be arbitrarily thick. A tungsten loaded epoxy mixture would be suitable here since these mixtures can easily achieve acoustic imedances of 20×10^6 kg/m^2 sec (matching the silicon) and are quite lossy. (The implications of the finite thickness of the backing layer for low frequency applications of these structures will be described later.)

Summarizing the important characteristics of the basic PVF_2-Si transducer structure, we have:

1. Si forms a high impedance "rigid" backing for the PVF_2 causing it to be thickness resonant at the quarter-wave frequency.
2. Thin layers of epoxy, SiO_2 or other insulators between the PVF_2

and the Si will have only a small effect on the acoustic performance of the structure.

3. No front matching layer is required, although a waterproofing parylene layer would typically be used.

4. Tungsten-loaded epoxy is suitable for a backing layer and is simple to use.

5. The sensitivity and bandwidth of the structure are comparable to that achieved by discrete PVF_2 transducers with brass backing layers [4].

6. The flexibility of PVF_2 films allows them to easily conform to a silicon wafer which may be slightly warped following high temperature processing.

The presence of a high performance semiconductor intimately connected to the PVF_2 transducer makes it possible to place one or more active devices directly behind each PVF_2 transducer. This may be done on a unit cell basis for linear or area arrays, making possible true batch fabrication of these transducer assemblies.

A purely capacitive load on the PVF_2 transducer is optimum (essen-

because of charge division between the transducer capacitance and load capacitance). A convenient means of achieveing this is to use as the bottom electrode of the PVF_2 transducer, the gate electrode of a Mosfet transistor as shown in Fig. 3. This forms a piezoelectric-oxide-semiconductor field effect transistor or Posfet. Acoustic waves hitting the top surface of the Posfet will induce a charge on the lower metal electrode which can then be used to modulate the conductivity of the underlying Mosfet channel.

There is one potential complication with the Posfet structures described to this point. This problem is illustrated in Fig. 4. (The dimensions given correspond to early experimental structures fabricated in the Integrated Circuits Laboratory.) As shown in the figure, the amplifier typically occupies only a small portion of the area of each cell. (The total cell area would likely be on the order of 10 mm^2 for acoustic imaging applications while the amplifier itself would occupy about 5% of the cell

area). The remainder of the cell is occupied by the lower aluminum electrode. Based upon this structure, the equivalent circuit in the figure may be drawn.

In this equivalent circuit, the 170 pf capacitor represents the parasitic capacitance between the lower aluminum electrode and the silicon substrate. We can estimate the value of the capacitors by noting that both SiO_2 and PVF_2 have approximately the same dielectric constant (3.9 for SiO_2 and approximately 6 for PVF_2 in the 1-10 MHz frequency range). For any arbitrary cell area, then, the PVF_2 transducer capacitance and the parasitic capacitance will be related by the respective thicknesses of the PVF_2 and SiO_2 layer. In addition to the parasitic capcitance to ground beneath the lower electrode, a second parasitic exists in the structure due to the finite thickness of the nonconductive epoxy used to physically attach the PVF_2 to the silicon wafer. For the early structure illustrated in Fig. 4, this capacitance has a value on the same order as the PVF_2 capacitance.

The net result of both of these effects is an approximately 15 times reduction in sensitivity of the simple structure shown here, below that intrinsically achievable with the PVF_2 structure. This situation clearly must be eliminated if practical transducers are to be fabricated. More will be said about this later.

II. ANALYSIS AND MODELING OF THE POSFET TRANSDUCER

The electrical port of the PVF_2 transducer may be modeled in the ideal case as a Trevin voltage source and series output imedance. The Thevenin voltage generator can be determined as a function of the input acoustic stress using the standard thin plate "thickness" mode Mason model [7]. The transducer, as described earlier, has a backing with acoustic impedance much greater than

that of the PVF_2. Therefore, the model of Fig. 5 applies. This lumped parameter circuit model of the transducer can be solved to give the relation

$$\frac{V_{out}}{T_{in}} = \left(\frac{2h}{jw}\right)\left\{\frac{1}{Z_w[1 - (j\bar{Z}_0/Z_w)\cot(\bar{B}\ell)]}\right\} \qquad (1)$$

Resonance occures when $\bar{B}\ell = \pi/2$, or $\ell = \lambda/4$. A ceramic transducer could be operated in the $\lambda/4$ resonant mode only with great difficulty because of the high acoustic impedance of the ceramic materials. As a result they are normally backed with a material of lower acoustic impedance, in contrast to PVF_2, and operate near the $\lambda/2$ thickness resonance. This mode is inherently less sensitive to low frequency excitation. The reduced bandwidth in the $\lambda/2$ mode can be regained partically be adding a matched acoustic backing to the ceramic transducer, at a cost of a substantial reduction in sensitivity. Figure 6 shows a normalized computer calculation of the voltage/stress transfer relation for a PVF_2 $\lambda/4$ transducer, resonant at 17 MHz, and for a typical 5MHz $\lambda/2$ ceramic transducer with a matched heavy backing for broadbanding, operating into a matching electrical load. Both curves apply for thin plate operation. Observe that, despite the lower electro-mechanical coupling coefficient k_T of the PVF_2 material relative to the ceramic (0.19 [2] vs. 0.49 [8]), the PVF_2 transducer provides greater acoustic sensitivity. The ceramic transducer sensitivity is reduced not only by the heavy backing but also by the inherent, acute acoustic mismatch between the ceramic and water. PVF_2, with much lower acoustic impedance, comes closer to a match with any liquid environment. Note that a PVF_2 transducer will have a sensitivity and bandwidth superior to a ZnO transducer (with k_T = 0.29 and Z = 36 x 10^6 kg/m^2-sec) for the same reasons.

The The edir series output impedance below resonance for the PVF_2 transducer can be calculated from Fig. 5. This gives

$$Z_{out} = \frac{(1 - k_T^2)}{jwC_0} \qquad (2)$$

where in terms of the material stiffness c_{33}^E, the piezoelectric stress constant e_{33}, and the dielectric constant ε_{33}^S,

$$K_T^2 = \frac{e_{33}^2}{c_{33}^E \varepsilon_{33}^S + e_{33}^2} << 1$$

Thus, the equivalent output impedance is simply a capacitor of value C_0 (to first order). Now, the importance of the MOSFET loading of the PVF_2 layer, inherent in the POSFET structure, becomes clear. Because of the negligible resistive loading by the MOS transistor, the ideal POSFET structure, including glue bond, may be modeled as shown in Fig. 7. We have

$$\frac{V_G}{V_{out}} \quad \frac{C_0 C_B}{C_0 C_B + C_0 C_{GSub} + C_B C_{GSub}} \tag{3a}$$

If the capacitance of the glue bond (C_B) is ignored, then

$$\frac{V_G}{V_{out}} = \frac{C_0}{C_0 + C_{GSub}} \tag{3b}$$

This relation is valid from dc to just below resonance. Furthermore, we have seen that, over this same frequency region, the Thevenin voltage generator V_{out} is nearly a constant and independent of frequency. Thus, with the commercially available 30 μm thick PVF_2, the POSFET structure offers the possibility of a frequency response flat within 6dB from dc to 17 MHz and a sensitivity comparable to or greater than a broadband ceramic transducer used in the same mode. Observe from Eq. (3b), however, that this full sensitivity cannot be realized unless the extended gate electrode capacitance (C_{GSub}) is minimized.

Of fundamental importance is knowledge of the absolute device detectivity

or minimum detectable signal level. This can be calculated for the PVF_2 transducer by modeling it electrically as a series real and imaginary impedance. The minimum detectable input acoustic power, then, is defined to be that which generates a Thevenin output voltage equal to the thermal noise voltage generated by the series real impedance. The principle source of thermal noise in a typical broadband ceramic transducer is due to coupling to the heavy backing used for broadbanding. This is not a problem for a PVF_2 transducer. However, dielectric loss within the PVF_2 at frequencies above 1 MHz is responsible for considerable noise. The result is that typical minimum detectable acoustic intensities are on the order of 5×10^{-11} W/cm^2 for PVF_2 with a 1 MHz bandwidth and a 1 mm^2 area. This is a factor of approximately two worse than that for the broadband ceramic transducer. This result was obtained for 30μm thick PVF_2. Better detectivities can be obtained by using thicker layers [9].

Additional reductions in detectivity arise, naturally, from the POSFET amplifier characteristics. Because of the integrated structure of the device, however (implying, for example, the absence of long electrical leads), the net transducer-amplifier detectivity for the POSFET may easily surpass that of a comparable ceramic transducer-amplifier system.

III. LOW FREQUENCY CONSIDERATIONS IN PVF_2 AND POSFET TRANSDUCERS

The plots in Fig. 6 indicate that the $\lambda/4$ resonant PVF_2 transducer responds to an acoustic input at dc. Initially, the following fundamental assumptions underlying the predicted broadband response described above should be reviewed before discussing low-frequency PVF_2 operation.

* In the "thin plate" Mason model in Fig. 5, the transverse dimensions of the transducer were assumed to be very large compared to an acoustic wavelength so that the lateral strains were zero.

* Vertical incidence of the acoustic wave was assumed; however, in the case of nonvertical incidence, substantial deviation

from simple theory results.

* Because the resistive part of the electrical load was assumed to be much less than the reactive component, a frequency-independent capacitive-divider relation [Eq. 3] expressed the electrical transfer characteristic.

* An infinitely thick or lossy acoustic backing was assumed.

Figure 8 is a schematic of a more accurate low-frequency model for the POSFET transducer, wherein the thin-plate Mason-model parameters in Fig. 5 have been replaced by the "narrow rod" values [7]. The thin-plate or thickness-extensional (TE) model assumes that the transducer has infinite transverse dimensions so that it is effectively clamped laterally, but this is an unacceptable approximation at very low frequencies. The narrow-rod model or length-expander bar (LE_p) assumes zero stress laterally (lateral dimensions$\ll \lambda$) and zero-impedance acoustic loading on the sides of the transducer. The new LE_p material parameters are quantitatively characterized by lower acoustic velocity and impedance and a higher coupling coefficient.

Two additional changes are evident in Fig. 8. The first is that the backing of the transducer is now a length of acoustic transmission line, followed by the acoustic impedance of the ultimate load which depends on frequency. At all except very low frequencies, the load is the acoustic medium--air or water. At the lowest frequencies, the load inpedance must include the effect of the mechanical clamp holding the transducer. The second change is the addition of a parallel resistor representing the high but finite POSFET biasing component R_1.

The narrow-rod model is one-dimensional, just as is the higher frequency thin-plate Mason model and, as a result, problems are encountered when the lateral dimensions are comparable to an acoustic wavelength. This was not considered in the preceding analysis because, although the electrode

width of each element was on the order of one wavelength, the dimensions of the array (consisting of a single PVF_2 sheet) were much larger. At frequencies where lateral dimensions compare to an acoustic wavelength, for example, coupling to the longitudinal-expander (LE_t) or planar-expander (PE) mode occurs; increased piezoelectric coupling and a corresponding reduction in bandwidth are expected at these frequencies. The flat V_{out}/T_{in} spectral response in Fig. 6 represents an uncoupled TE model which, in reality, is converted into a length expander (also flat) at very low frequencies, with ripples in the V_{out}/T_{in} response in the change-over region.

Another inaccuracy in the model employed above can also be seen in Fig. 8. The acoustic backing of the transducer is of finite thickness and impedance and, in the high frequency analysis above, they were assumed to be infinite. Because of the wave nature of sound, the backing actually should be a length of transmission line (capable of impedance transformation via wave reflection from its rear termination). At frequencies where the backing thickness is a multiple of $\lambda/2$, the PVF_2 reacts to the impedance of the medium (air or water) instead of to a high-impedance load; compression in response to an input wave will drop, and the piezoelectrically generated output voltage is reduced. This is illustrated in Fig. 9 where the output-voltage/input stress relationship of a PVF_2 transducer is plotted at low frequencies (calculated for a transducer with a high-impedance tungsten-loaded epoxy backing, 7/2 resonant at 10 kHz, in both ambient air and water). Low-frequency operation can be achieved despite these problems by applying very thick backings or by coupling to one of the lateral modes.

A nonacoustic source of concern is the electrical loading of the PVF_2 by the MOSFET bias resistor R_1. As in high-frequency operation, the PVF_2 output impedance is primarily its clamped capacitance. At low

frequencies where $R_1 < 1/\omega C_{GSub}$, the ratio of gate input voltage to Thevenin output voltage is

$$\frac{V_g}{V_{th}} = \frac{R_1 C_0 \omega r}{[1 + [R_1 \omega r (C_0 + C_{GSub})]^2 + 1]^{1/2}} \approx R_1 C_0 \omega r \quad (4)$$

The input pole at $\omega = 1/[R_1 (C_0 + C_{GSub})]$ should be located below the intended operating frequency. The resistance of R_1 can be increased by substituting a back-biased diode whose reverse-leakage current then supplies the necessary MOSFET input current. More advanced circuit techniques may be implemented at low frequencies.

The ideal PVF_2 "thin plate" mode of operation may be impractical at frequencies below 200 kHz. In addition, because low-frequency transducers are large-area devices, the dimensions of a monolithic array would be limited by the largest silicon dimensions. Powerful signal-processing electronics directly coupled to the transducer, however,is a significant advantage, independent of the acoustic mode of operation.

Many low-frequency applications for PVF_2 appear to be well suited for POSFET implementation. Among these are a medium-frequency (100 Hz to 100 kHz) sonar sensor or shock-wave detector for naval and underwater geological applications and a very low frequency "pressure" transducer. The V_{out}/T_{in} conversion factor yields an approximately 1.1 V output for a 1 atmospheric-pressure input, assuming that the PVF_2 is rigidly supported.

IV. EXPERIMENTAL RESULTS ON PVF_2 TRANSDUCERS AND POSFET ARRAYS AS RECEIVERS

Prior to the beginning of this contract, discrete elements and small linear arrays of POSFET transducers, using the technology illustrated in

Fig. 4, were fabricated with commercially available 30μ thick PVF_2. Photographs of a single element and a three element linear array (both before the PVF_2 layer is attached), are shown in Fig. 10. When used in a liquid medium, these transducers are predicted to have a frequency response essentially flat from DC to greater than 10 MHz. It is difficult to measure such a response because of the absence of a transmitting transducer with comparable characteristics. However, when a commercial broadband, 5 MHz, ceramic transducer (the Panametrics VIP- 5-1/2I) is used as a transmitter, the pulse response shown in Fig. 11 is obtained. This response is essentially limited by the transmitting transducer, showing that the PVF_2 bandwidth is far greater.

Details of the frequency response illustrated in Fig. 11 are shown in Fig. 12. It is quite clear that the high frequency response is limited by the Panametrics ceramic transmitter; the apparent low frequency roll-off of the Posfet device is a result of the package in which the device was placed and is not intrinsic to the Posfet.

Far-field radiation patterns of the linear array have been made, as shown in Fig. 13, which show that array inter-element cross coupling, while present, will not substantially degrade array performance. Receiver sensitivity of this device is at least as good as that of the Panametrics transducer, except for the factor of 14 degredation due to C_{Gsub} (Eqn. 3).

In parallel with the transducer fabrication and analysis on this contract we have also continued to develop complete integrated arrays for higher frequency use. Since the fabrication techniques, circuit designs, mechanical assembly and resultingperformance are very relevant to the low frequency applications considered here, we briefly summarize below the significant results of this array investigation.

The highlight of this work has been the successful demonstration of a 34 element linear array with integrated per unit cell amplifiers [10]. The

basic cascode amplifier of Fig. 14 was used in each cell of the array. It has a midband gain of 12, a 3 dB bandwidth of 5 MHz, delivers 1.4 V_{p-p} into a 100 pF output load, and dissipates 15mW. It makes use of an input double-diffused MOS transistor (DMOS) to increase the device transconductance without increasing area, by reducing the channel length, L [11]. Typical channel lengths of 1.5 to 2.5μm are obtainable for this transistor.

In this circuit, R_1 supplies bias current to the MOSFET gate. Because it determines the low-frequency roll-off of the response, it is made as large as possible. R_2 determines the gain of the amplifier and R_3 establishes the dc current flow in the output stage, thus determining the output drive capability. V_1 biases the MOSFET at the desired operating gate voltage, V_2 sets the dc drain-source voltage for the MOSFET so that it is operated in saturation, and V_3 is the main supply, providing output and cascode bias current.

The amplifier is fabricated within an n-type epitaxial layer grown on a p-type silicon substrate. A photomicrograph is shown in Fig. 14b. All of the components in the amplifier are isolated by conventional p-type diffusions. Cross-sectional diagrams of the active components are shown in Fig. 15. The DMOS transistor has a drain and channel region folded around a central source, giving a channel width of 500μm, for an expected minimum Z/L of 200. The NPN bipolar transistors are small geometry, vertical devices. R_1 is a pinched epitaxial resistor with a length to width ratio of 10, giving an expected 100 kΩ resistance. R_2 is an epitaxial resistor of 6.4 kΩ. R_4 is a 20Ω, n^+ diffused resistor.

Similar power supply, bias voltage, and ground lines are bussed across the array in order to minimize the number of external connections. As a result, only an output connection is required for each amplifier. Four additional connections are needed for V_1, V_2, V_3, and ground. In future designs all of the supply voltages may be derived on-chip from a single external

supply.

Most of the cell area is occupied by the DMOS extended gate electrode. A thick field oxide (~1.5μm) is grown over the expitaxial layer, and aluminum is deposited on this oxide. This region is isolated from the adjoining amplifier by a p^+ isolation diffusion, and the epitaxial layer is allowed to electrically float. This places the isolation-epitaxial layer junction capacitance in series with the oxide capacitance, so that C_{GSub} is reduced.

A photomicrograph of the array is shown in Fig. 16. The individual element dimensions are 0.42 mm x 9.0 mm. The center 0.37 x 7.0 mm of each device is occupied by the extended gate electrode detector. Amplifiers of adjacent elements alternate sides on the array, simplifying the problem of making external output connections and reducing electrical cross-coupling.

The devices were fabricated in 12 μm 3Ω-cm, As doped epitaxial layers on p-type, (100), 5-10Ω-cm silicon substrates. The fabrication steps are summarized below.

* P^+ isolation predep and drive-in.
* P^+ channel contact and extrinsic base predep and drive-in.
* P^- channel and intrinsic base implant. N_2 drive-in to prevent oxide growth.
* N^+ source, drain, and emitter predep and drive-in.
* Gate oxidation.
* Contact hold opening.
* Metal deposition and definition.
* SiO_2 passivation.

The only step which must be carefully controlled in the process is the p^- implant because it largely determines both DMOS threshold voltage and NPN current gain. Typically a dose of $7 \times 10^{13}/cm^2$ @ 50 KeV is used, resulting in a DMOS threshold votage V_T of approximately +1 V. The bipolar base is defined by the same double-diffused profile that determines the DMOS channel length. The

use of a relatively long channel (and therefore wide base) makes threshold voltage control substantially easier in the DMOS transistor [11]. Low bipolar β which is typical of the DMOS process used, was compensated in the circuit design through the use of a Darlington pair.

The very large size of the silicon chip necessitated the construction of a custom substrate. Selected for this purpose was Dow Corning "Fotoform" glass. This material, with acoustic impedance of 13.5×10^6 kg/m^2-sec, is photosensitive and etchable, so that the eight-sided polyhedral shape and pattern of small connection holes could be formed by masking and chemical etching. A 1500 Å titanium-tungsten composite, followed by 4500 Å of gold, were sputtered onto the glass. The titanium provides adhesion to the glass, while the tungsten prevents formation of titanium-gold intermetallics, and the gold layer supplies most of the current conduction capability. Following definition of the metal pattern on the substrate by means of standard masking techniques, and a two-stage metal etch, the substrate is ready to serve as a mount for the silicon array.

Completion of the array in preparation for detailed acoustical and electrical measurements proceeded as follows.

1. The silicon die were separated into discrete arrays using a diamond saw.

2. Individual die were glued to the glass substrate using conductive epoxy.

3. Wire bond connections were made between the power supply and amplifier output pads, and the corresponding pads on the glass substrate. Figure 17 is a photgraph of the array at this point.

4. A heavy rectangular backing composed of Emerson and Cuming Stycast 1217 epoxy, loaded with tungsten particles, was cast on the back-side of the array, directly below the silicon die. The acoustic impedance of this backing was chosen to match that of the silicon ($\sim 23 \times 10^6$ kg/m^2-sec) to prevent reverberation.

5. External wire connections were inserted through the holes in the glass substrate from the rear and epoxied to the gold connection pads, again using the two-part conductive epoxy.

6. A 14.7 x 7.0 mm sheet of 30 μm PVF_2 was glued to the central surface of the silicon die, using Stycast 1217. Ground connections were made to the upper aluminum electrode of the PVF_2 at two diagonally opposite corners using conductive epoxy.

7. A 10 μm layer of Parylene, a monomer plastic coating, was deposited to act as a moisture barrier for the exposed upper aluminum electrode and wire bond connections.

The prototype is shown mounted in Fig. 18.

The output voltage/input stress transfer relation for the array was measured and is plotted vs. frequency in Fig. 19. The voltage gain of the amplifier is contained within this measurement. Therefore, the frequency characteristic is essentially that of the PVF_2 (Fig. 6), multiplied by the amplifier response. When the amplifier gain and the gate voltage divider ratio are factored out, the PVF_2 transfer amplitude is approximately 0.15 V-cm_2/N, independent of frequency, vs. 0.11 predicted from Fig. 4. Resonances are largely absent because of the use of a thick and lossy backing.

The impulse response was obtained by driving a discrete PVF_2 transmitting transducer with a current impulse. A water medium was used between the transmitter and the array. This impulse and the array output signal are shown in Fig. 20. It is seen that the response has decayed 20 dB below the peak after 0.3 μsec. This translates to an axial resolution in water of 0.3 mm, which is considerably superior to the best obtainable from 2 to 5 MHz ceramic transducer arrays in medical imaging applications, where the elements are physically separate and lateral resonances can be a severe problem. The monolithic nature of the POSFET array is responsible for this superior impulse response.

In order to evaluate experimentally the performance of PVF_2 transducers at low frequencies and to verify some of the theoretical calculations on low frequency behavior described above, a series of transducers were prepared in the Integrated Circuits Laboratory for NRL. To unambiguously evaluate the PVF_2 material properties and the influence of mounting structures at these frequencies, these transducers did not contain any active electronics.

The actual evaluation of the tranducers was performed at NRL in Orlando because of specialized equipment available there. The details of this evaluation are contained in an NRL report by Yoram Berlinsky [12] and will be summarized here.

The structure of the transducer samples is shown in Fig. 21 (taken from Y. Berlinsky's NRL report). Sapphire substrates were used because of their mechanical strength and because of their compatibility with silicon on sapphire integrated electronics. (SOS technology is regarded as the most promising technique for eliminating C_{GSub} and hence improving Posfet sensitivity in future arrays.) The sapphire substrates were metallized with Ni which was photographically defined as shown in the figure. PVF_2 samples from Kureha (27μm thick) were then prepared as follows:

1. The aluminum electrodes supplied by Kureha were chemically removed. (First attempts to fashion reliable wire connections to these electrodes were unsuccessful because of peeling of the aluminum for the PVF_2.
2. Chrome-gold electrodes were sputtered into the PVF_2 by Professor John Shaw's group in the Ginzton lab at Stanford.
3. Repoling of the PVF_2 films was accomplished in the Center For Materials Research at Stanford. (This was necessary because of the elevated temperatures and electric fields involved in the sputtering process.
4. 1 cm squares of the PVF_2 were cut and mounted on the nickel electrodes on the sapphire substrates with a non-conductive epoxy.
5. Connections were made to the upper electrode of the PVF_2 using conductive epoxy and gold wires.
6. Wires were attached to the nickel pads on the sapphire substrate and the entire assembly coated with parylene for waterproofing.

Measurements of the piezoelectric, mechanical and conversion efficiencies of these transducers were performed at the Underwater Sound Reference Division of NRL by Y. Berlinsky over the range of temperatures and pressures appropriate to underwater applications. The following basic conclusions were reached.

1. The efficiency of the transducers corresponded to that expected theoretically. The use of a non-conductive epoxy to mount the PVF_2

on the sapphire results in a series capacitance between the transducer and lower Ni electrode. This slightly degrades the sensitivity; a conductive epoxy would eliminate the effect.

2. Resonances in the low frequency response characteristic were observed due to the sapphire substrate. These were eliminated through the use of a heavy metal backing behind the sapphire, resulting in a flat, low frequency response between 50Hz and 2kHz.

3. Measurements of PVF_2 transducers under conditions of very high stress fields demonstrated their superiority in some respects to ceramic transducers, particularly in their ability to tolerate high stress fields.

In summary, these measurements and those performed at higher frequencies at Stanford have confirmed the suitability of PVF_2 for a number of underwater hydrophone applications and suggested directions for future work in integrated PVF_2 / SOS transducers and arrays.

V. CONSIDERATIONS RELATING TO THE USE OF PVF_2 AS A TRANSMITTER

The most functionally flexible piezoelectric transducer is one which can be used both for transmission and reception of acoustic energy. PVF_2 has received little consideration as a transmitter of acoustic energy in the past because of its low electromechanical coupling coefficient, low dielectric constant and high dielectric loss. An analysis of its transmission capabilities and experimental confirmation of the results is of interest, however, and has been performed under the contract.

A technical paper describing this work has been prepared and submitted to IEEE J. Sonics and Ultrasonics. This paper is included in this report as Appendix 1.

VI. SUMMARY AND CONCLUSIONS

This report has considered the use of PVF_2 acoustic transducers in the

low frequency range of interest to underwater applications. Theoretical analyses of the expected performance of simple PVF_2 transducers and integrated silicon - PVF_2 (Posfet) transducer arrays at both high frequencies and low frequencies have been carried out and verified experimentally. Fabrication techniques for monolithic silicon arrays and sapphire based transducers have been developed. Experimental transducers have been fabricated; their performance verified the theoretical models which were developed.

REFERENCES

[1] Bui, L., H.J. and Zitelli, L.T., "Study of Acoustic Wave Resonance in Piezoelectric PVF_2 Film," IEEE J. Sonics and Ultrasonics, Vol. SU-24, No. 5, Sept. 1977, pp. 331-336.

[2] Ohigashi, H., "Electromechanical Properties of Polarized Polyvinylidene Fluoride Fibers Studied by the Piezoelectric Resonance Method," J. Appl. Phys. 47, March 1976, pp. 949-55.

[3] Kawai, H., "The Piezoelectricity of Poly (Vinylidene Fluoride)," Japan J. Appl. Phys. 8, 1969, pp. 975-976.

[4] Bui, L. J.H. Shaw, and L.T. Zitelli, "Experimental Broadband Ultrasonic Transducers Using PVF_2 Piezoelectric Film," Electronics Letters, 12, 1976, p. 393.

[5] J.D. Plummer, R.G. Swartz, M.G. Maginness, J.R. Beaudouin, and J.D. Meindl, "Two-Dimensional Transmit/Receive Ceramic Piezoelectric Arrays: Construction and Performance," IEEE Trans. on Sonics and Ultrasonics, Vol. SU-25, No. 5, Sept. 1978, pp. 273-280.

[6] Settig, E.K., "Effects of Bonding and Electrode Layers on the Transmission Parameters of Piezoelectric Transducers in Ultrasonic Digital Delay lines," IEEE Trans. on Sonics and Ultrasonics, SU-16, Jan. 1969, pp. 2-9.

[7] D. Berlincourt, "Piezoelectric Crystals and Ceramics," Ultrasonic Transducer Materials, O.E. Mattiat, ed., Plenum Press, NY, 1971, Ch. 3, pp. 74-76.

[8] H. Jaffe and D.A. Berlincourt, "Piezoelectric Transducer Materials," Proc. IEEE, Vol. 53, No. 10, OCt. 1965.

[9] R.G. Swartz, Application of Polyvinylidene Fluoride in Monolithic Silicon/PVF_2 Transducer Arrays, Ph.D. dissertation, TR No. G651-1, Stanford Electronics Laboratories, Stanford University, Stanford, CA, June 1979, Chapter 4.

[10] R.G. Swartz, and J.D. Plummer, "Integrated Silicon - PVF_2 Acoustic Transducer Arrays" to be published in IEEE Trans. Elec. Devices, Dec. 1979.

[11] H. Sigg, G.O. Vendelin, T.P. Cauge. and J. Kocsis, "DMOS Transistor for Microwave Applications," IEEE Trans. on Electron Devices, Vol. ED-19, Jan. 1972, pp. 45-53.

[12] Y. Bar-Cohen, "Transduction With PVF_2 In the Ocean Environment" Naval Research Laboratory Report, Underwater Sound Reference Division, Orlando, Florida.

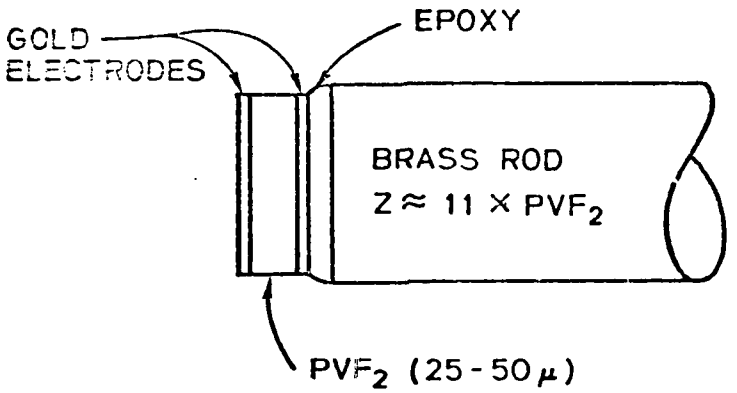

Fig. 1. Structure of Experimental Transducers Fabricated in Ginzton Laboratory.

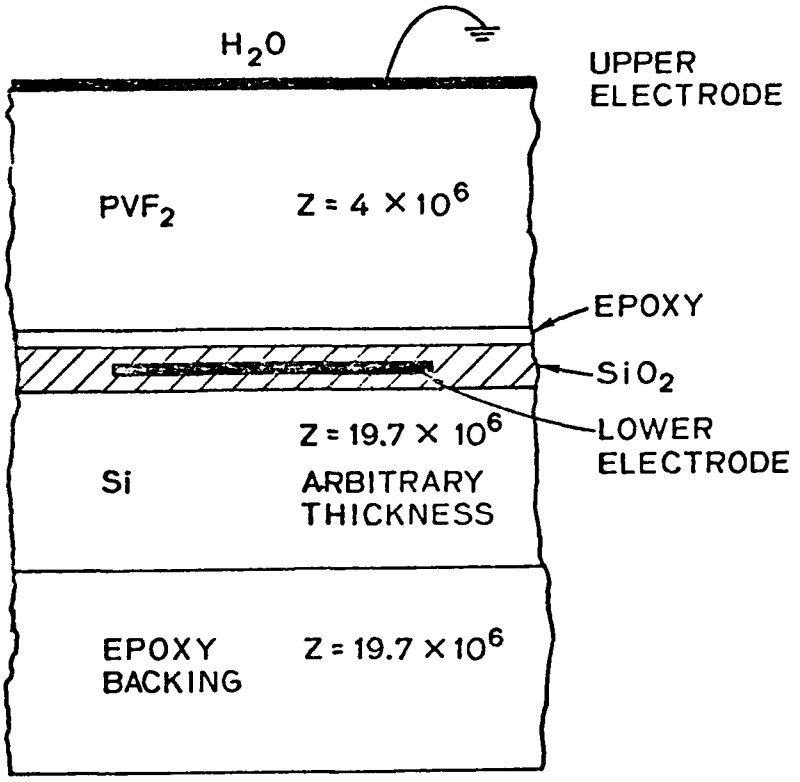

Fig. 2. PVF_2 Acoustic Transducer with Si Backing Layer.

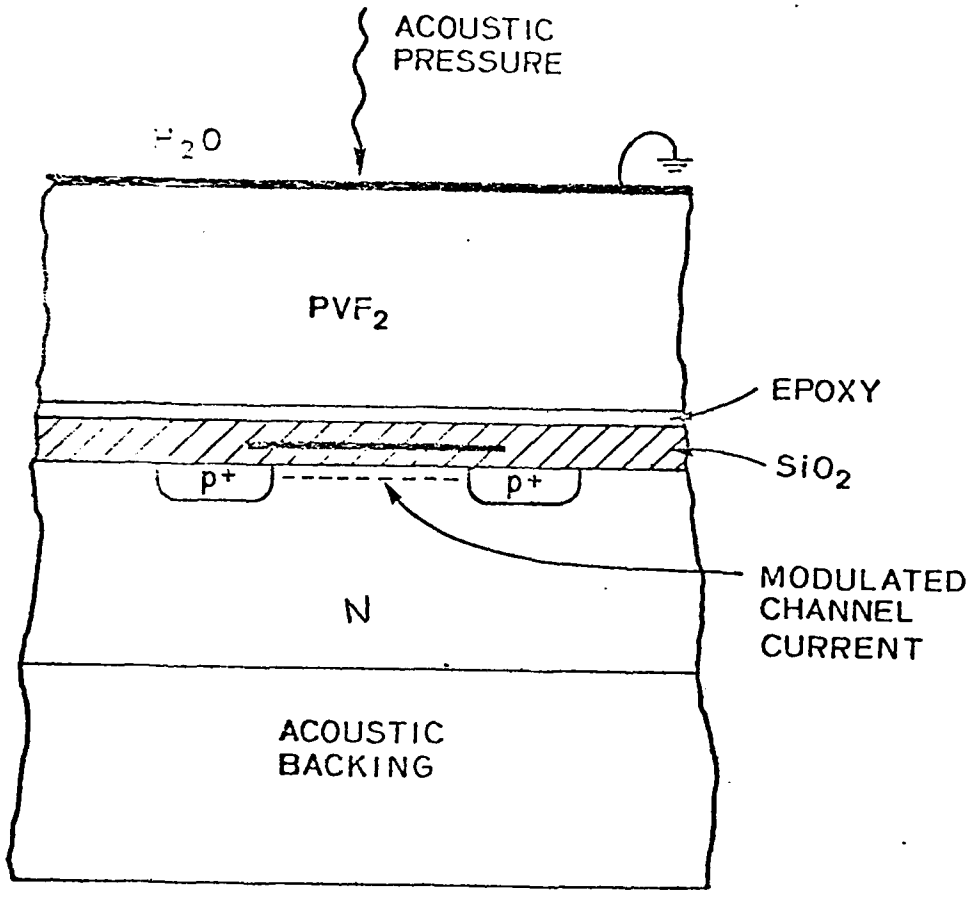

Fig. 3. Addition of an MOS Transistor to the Basic Posfet Structure.

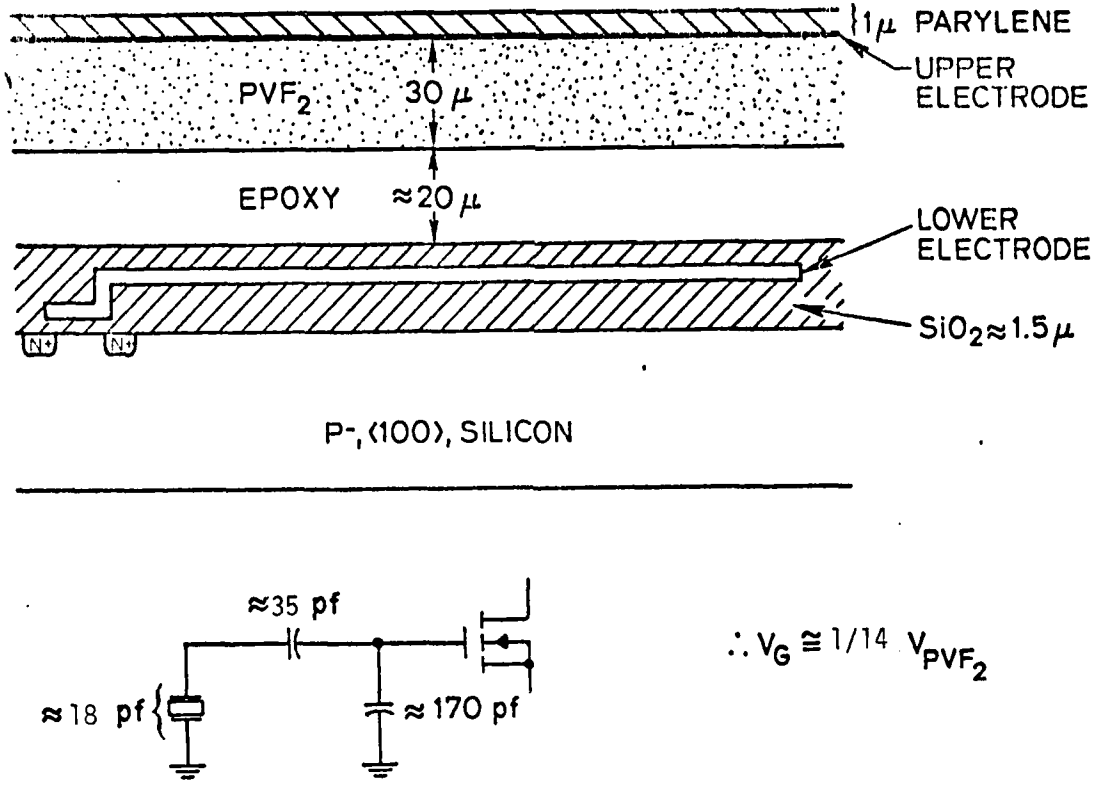

Fig. 4. Cross-Section of First Posfet Experimental Transducers Showing Origin of Parasitic Capacitances.

26

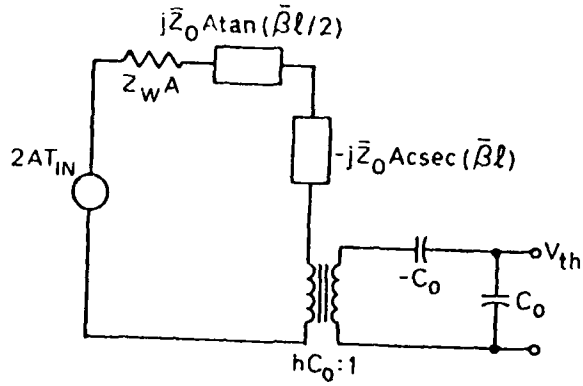

Z_w = acoustic impedance of water

A = surface area of transducer

T_{in} = acoustic input stress

ℓ = thickness of transducer

C_0 = clamped capacitance of transducer

$\bar{Z}_0$ = stiffened acoustic impedance of transducer

V_{th} = Thevenin equivalent output voltage

Figure 5. Mason Model equivalent circuit for the POSFET transducer.

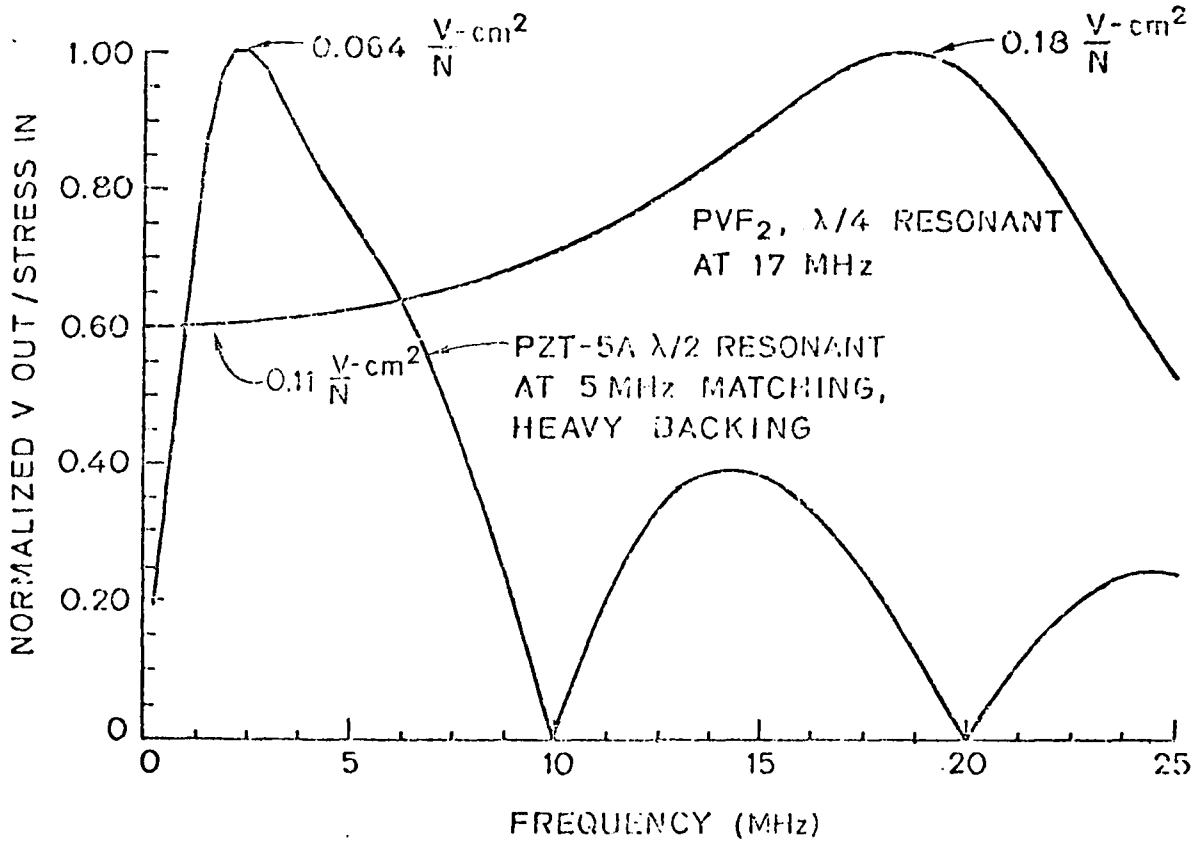

Figure 6. Output-voltage/input-stress transfer relationship vs. frequency for a broadband ceramic transducer (PZT) and POSFET.

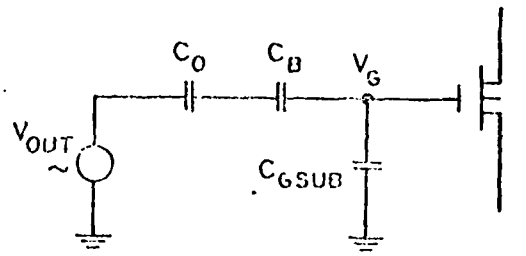

Figure 7. POSFET equivalent circuit.

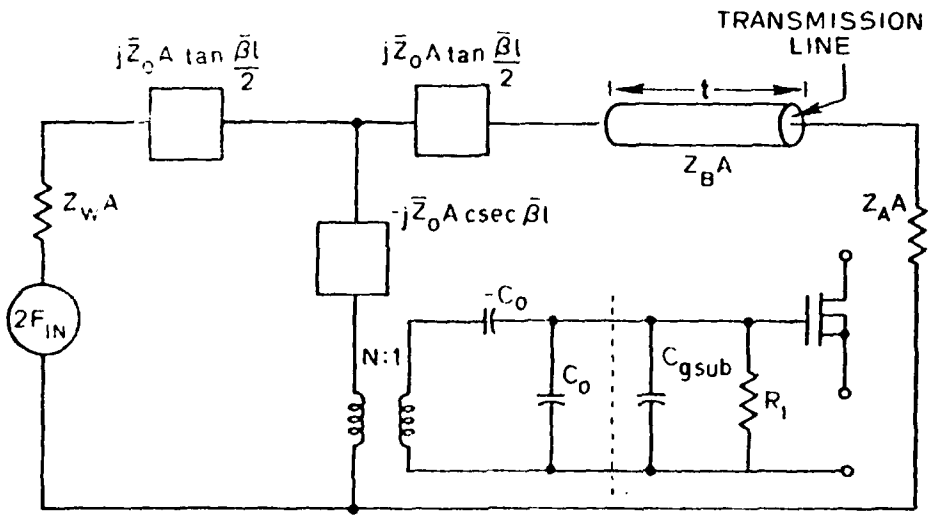

$C_0 = \epsilon_{33}^T A(1 - k_{33}^2)/\ell$

Z_W = specific impedance of water

Z_A = specific impedance of ambient

$\beta = \omega/v_a$

A = area

$\bar{Z}_0 = \rho \bar{v}_a$

$\bar{v}_a = (\rho S_{33}^D)^{-1/2}$

$N = Ag_{33}/\ell S_{33}^E \beta_{33}^T$

ℓ = thickness of transducer

t = thickness of backing

Fig. 8. LENGTH-EXPANDER MASON MODEL FOR DESCRIPTION OF THE POSFET AT LOW FREQUENCIES.

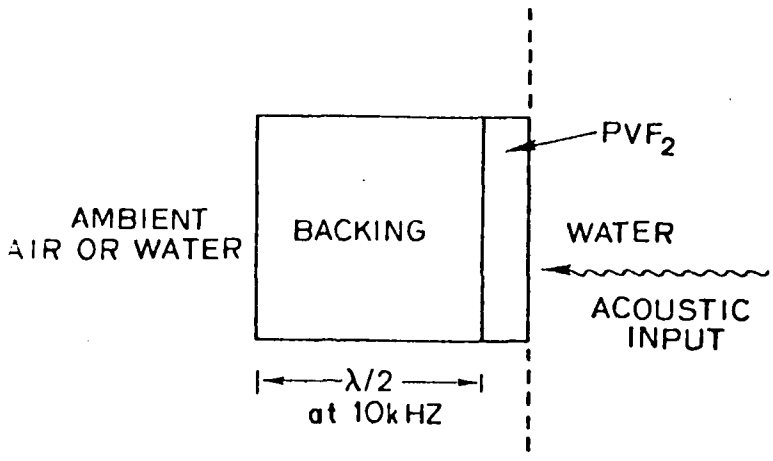

a. Cross section of transducer

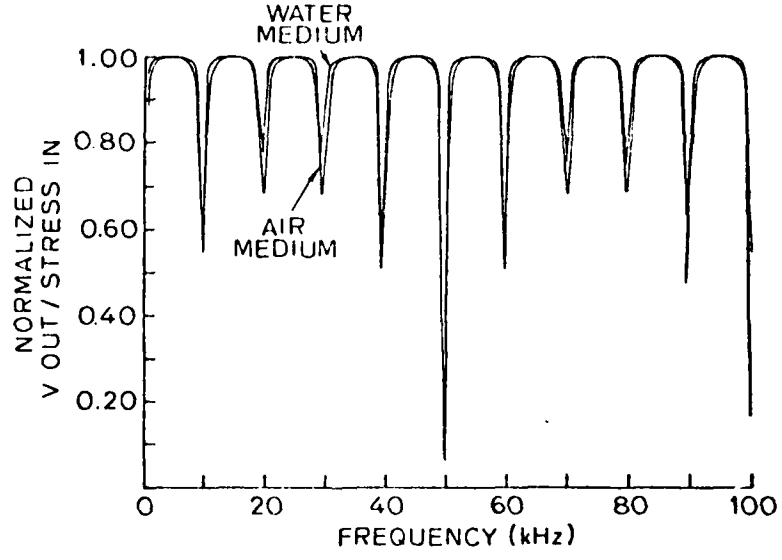

b. POSFET response at low frequency with shallow lossless backing (variation in depth of minima is an artifact of computer simulation)

Fig. 9. EFFECT OF FINITE-BACKING THICKNESS ON V_{out}/T_{in} TRANSFER RELATIONSHIP.

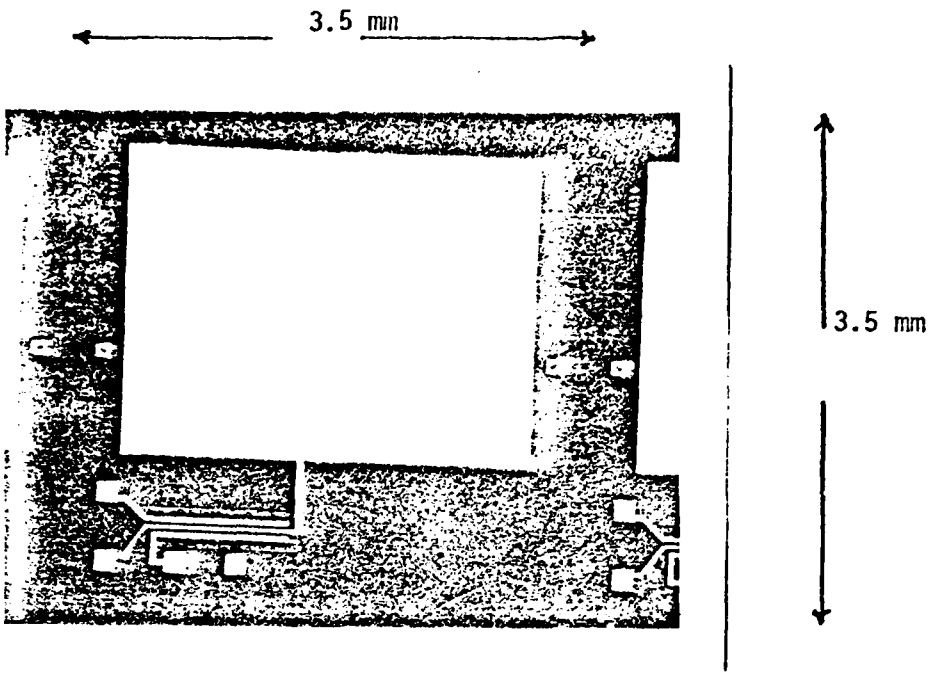

a) Portion of Si wafer containing single transducer cell. The large Al area is the lower electrode; the MOS transistor amplifier is in the bottom left corner.

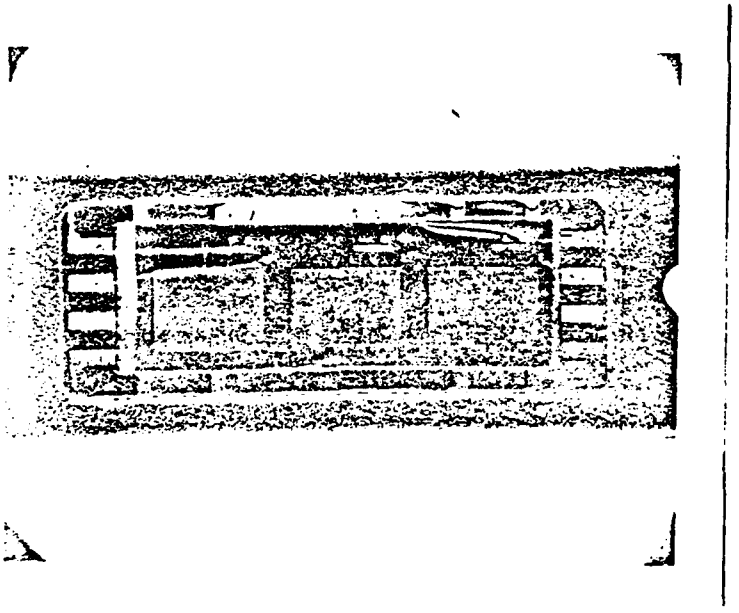

b. 3 element linear array of Posfet devices mounted in a standard dual-in-line package for experimental evaluation.

Figure 10.

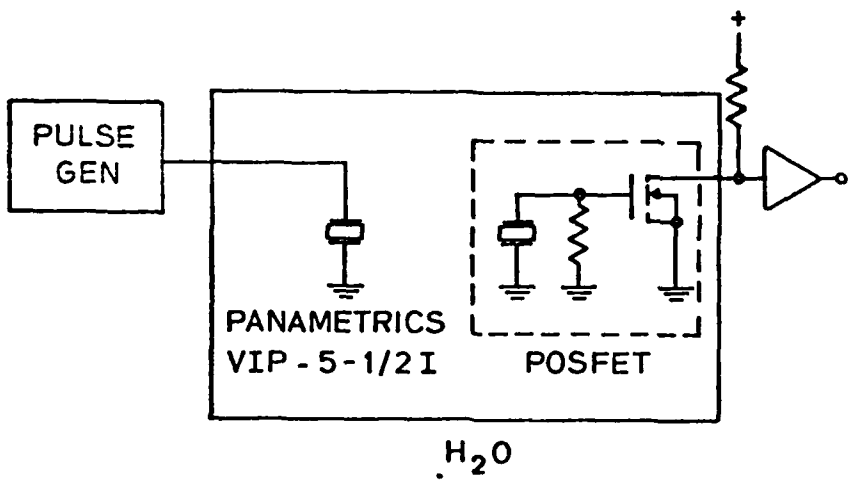

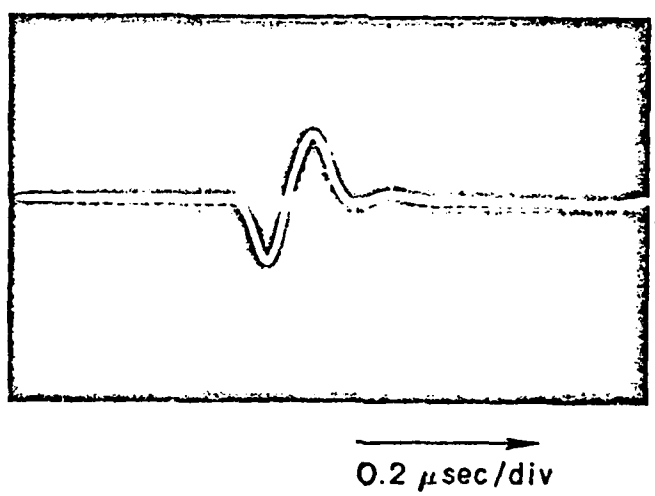

Fig. 11. Impulse Response of Posfet Transducer with Broadband Ceramic Transducer Used as Transmitter.

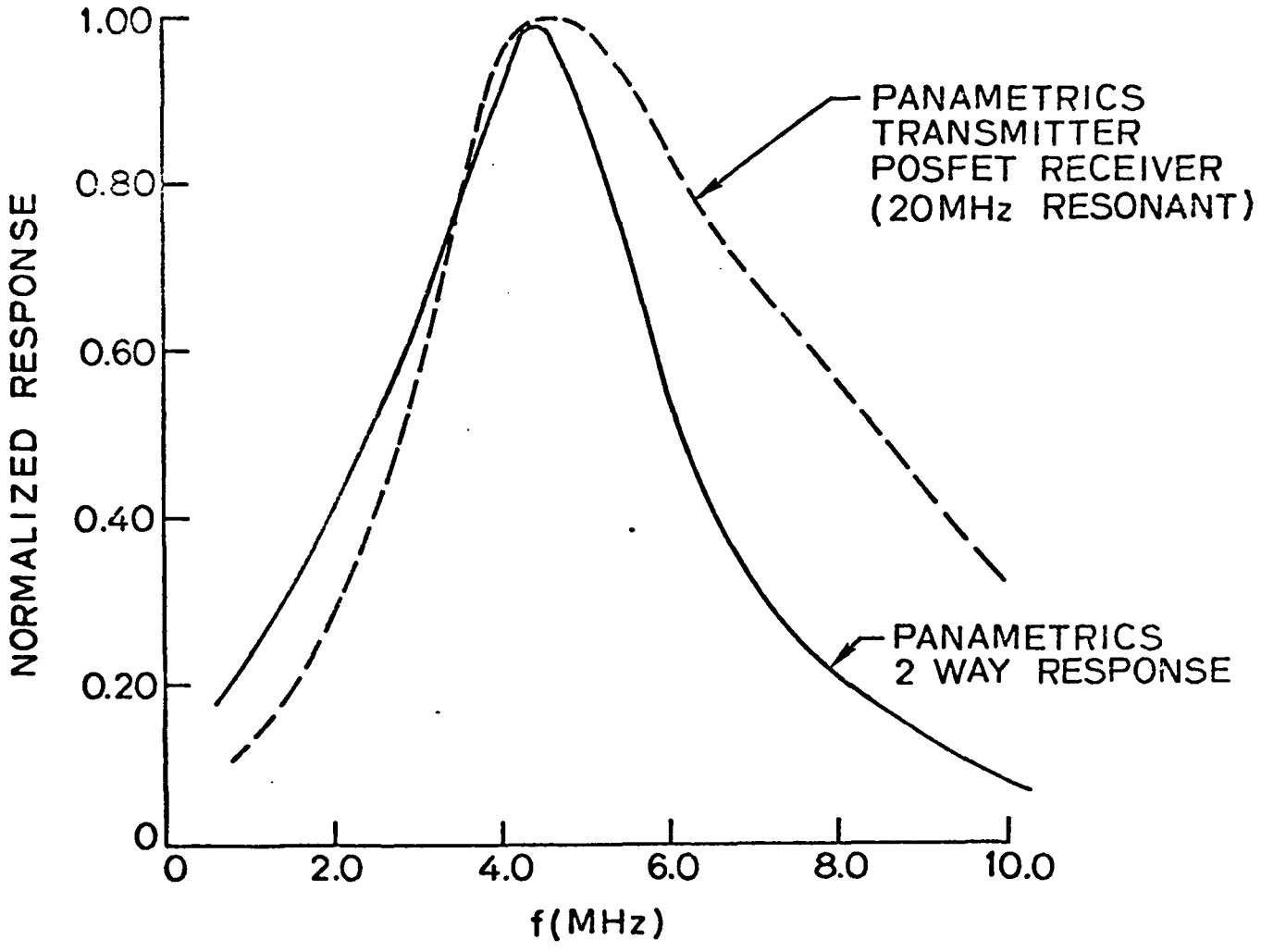

Fig. 12. Experimentally Measured Frequency Response of Posfet Receiver.

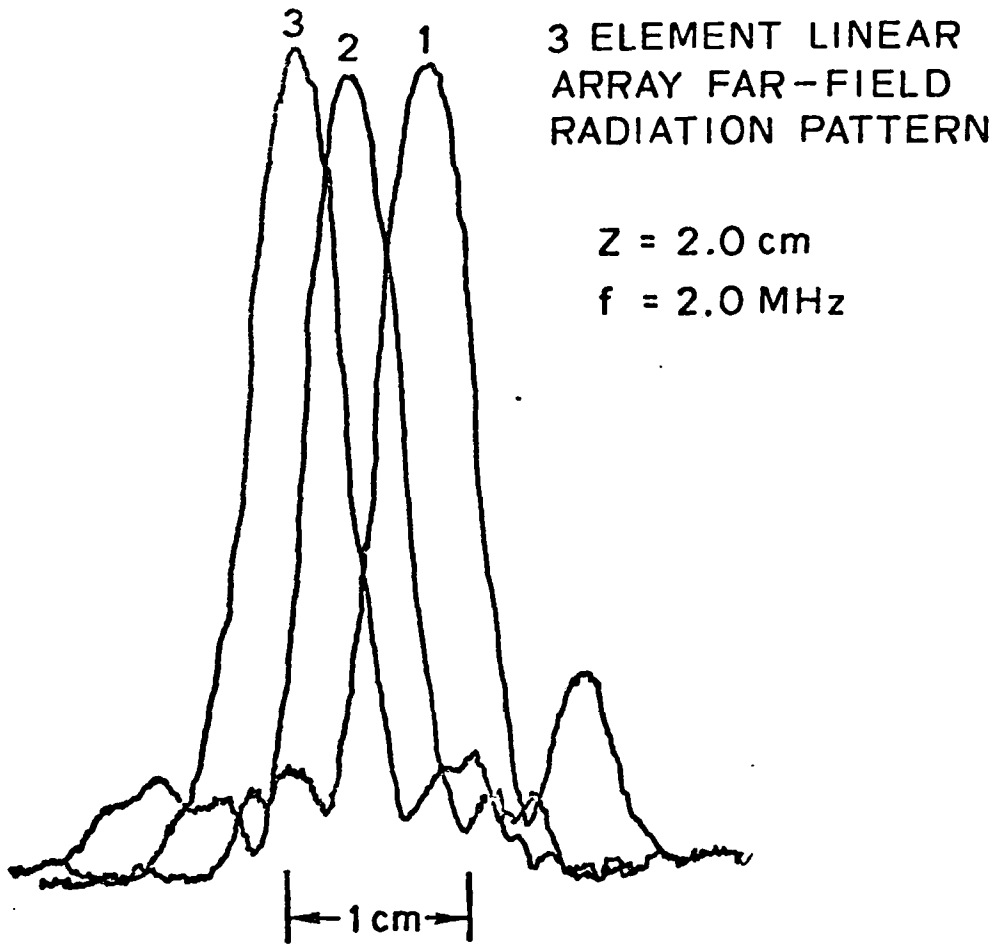

Fig. 13. Experimentally Measured Far-Field Radiation Patterns of Three Element Linear Array of Posfet Transducers.

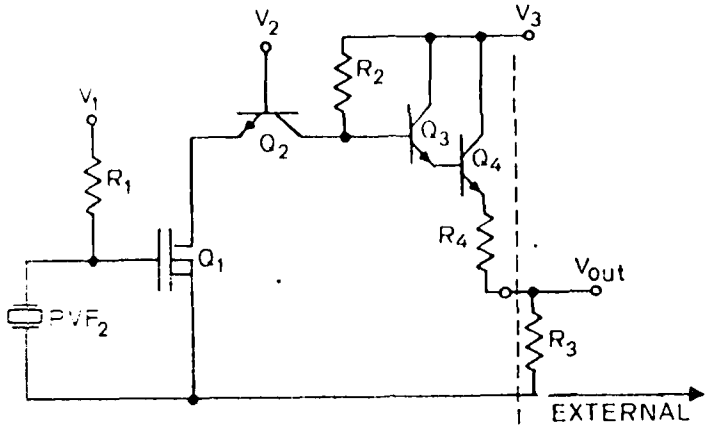

a. Schematic

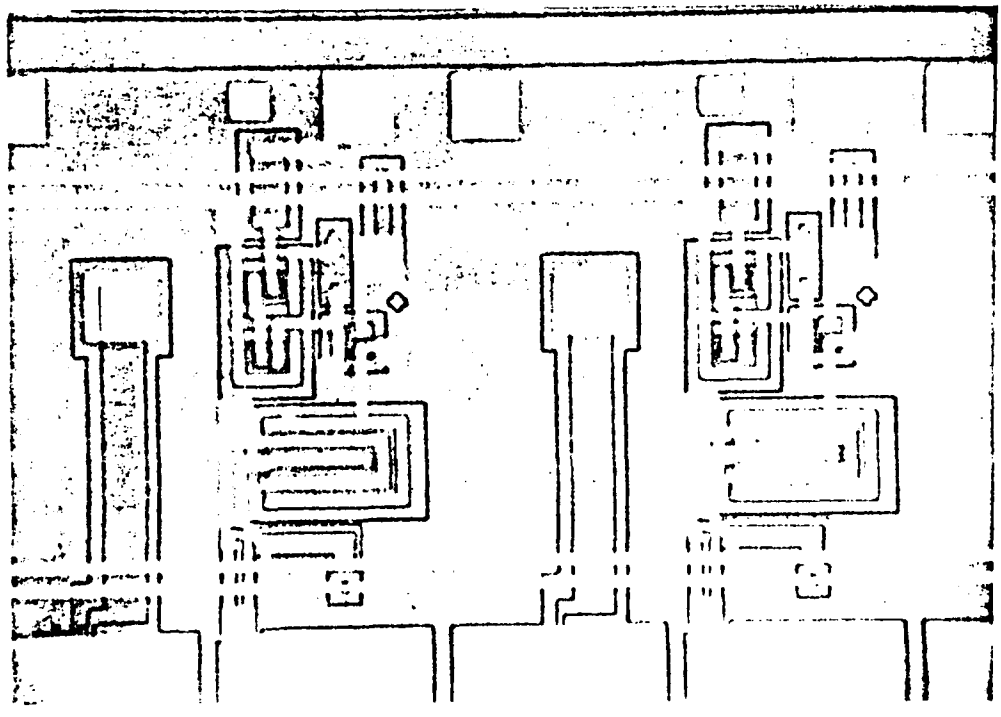

b. Photomicrograph

Figure 4. Integrated realization of the POSFET amplifier.
a. Schematic. b. Photomicrograph.

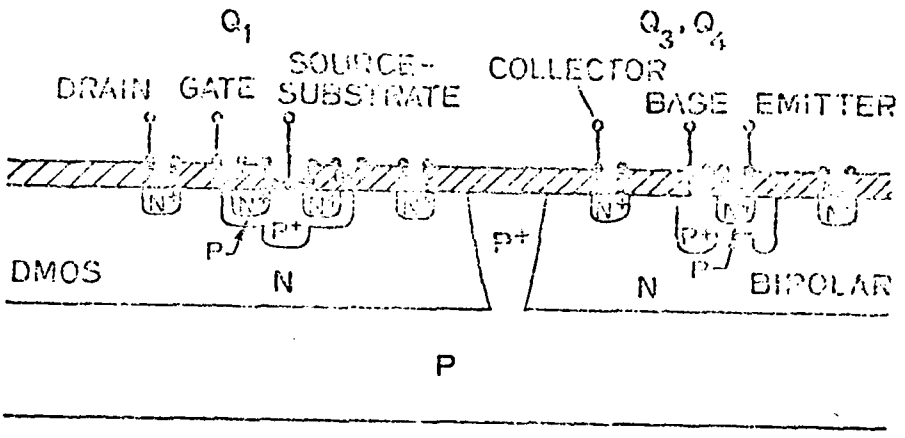

Figure 15. Silicon cross section of amplifier active components.

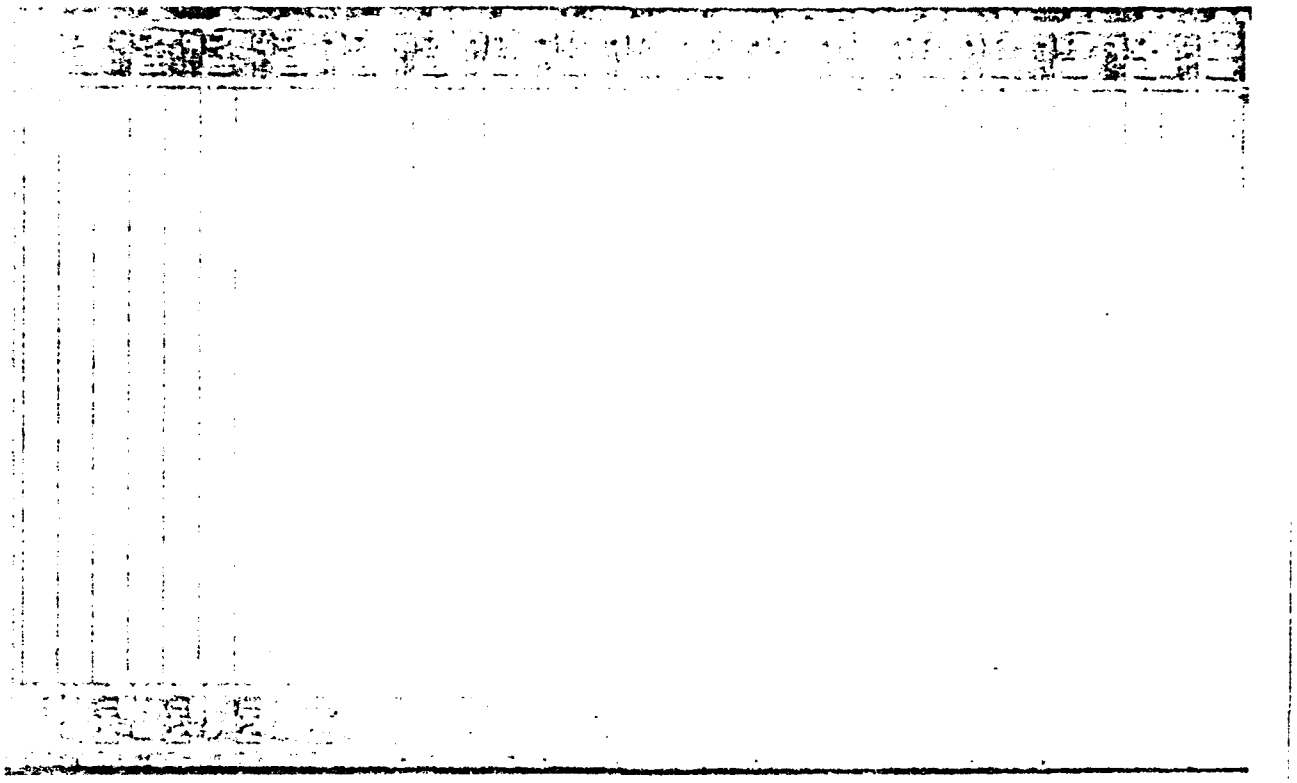

Figure 16. Photomicrograph of POSFET array.

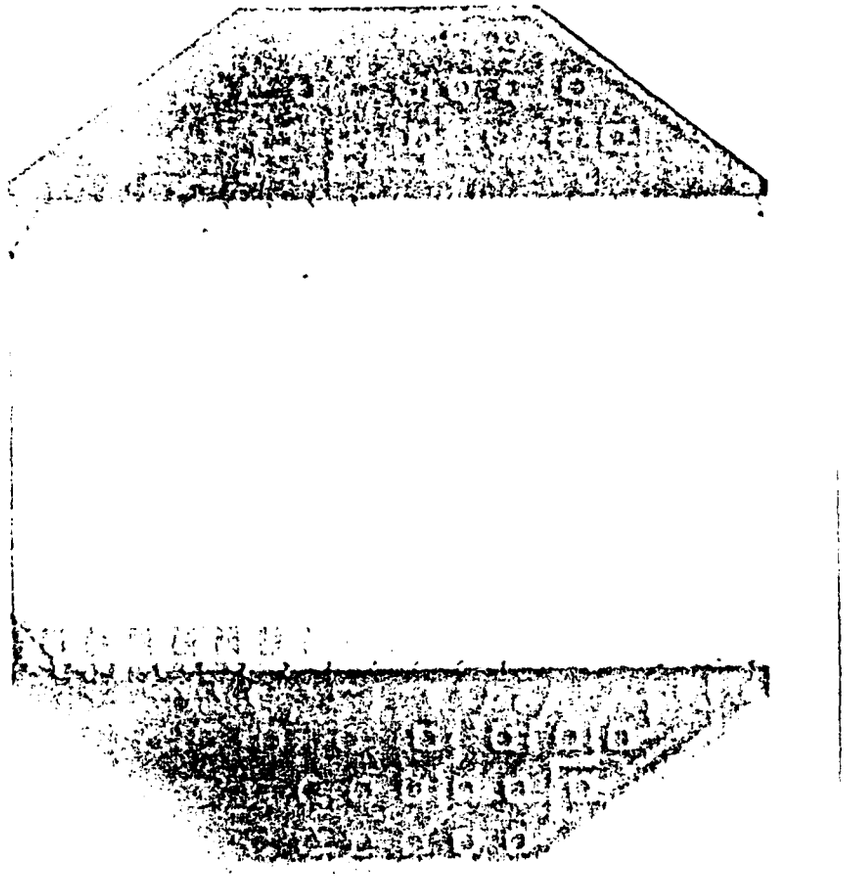

Figure 17. POSFET prototype after attachment of wire bond connections.

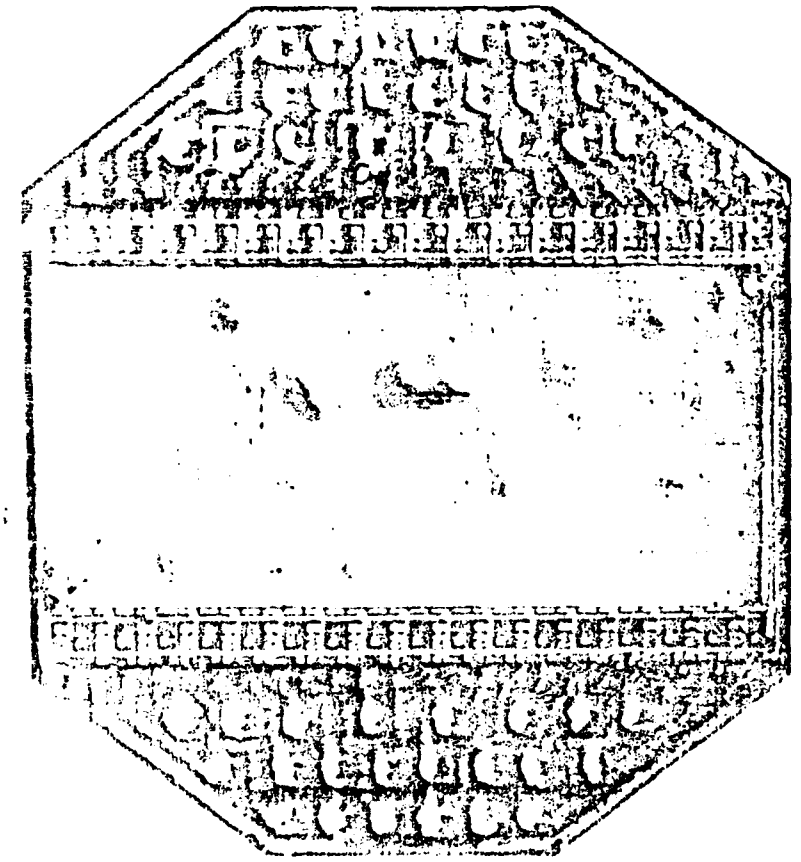

Figure 18. Mounted POSFET prototype array.

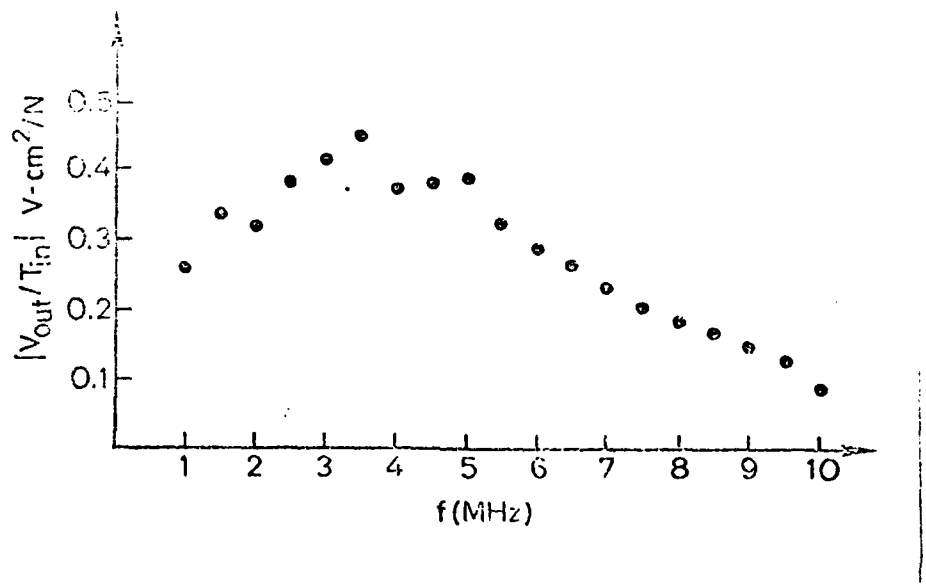

Figure 19. Measured output-voltage/input-stress transfer relationship vs. frequency of the POSFET array.

a.

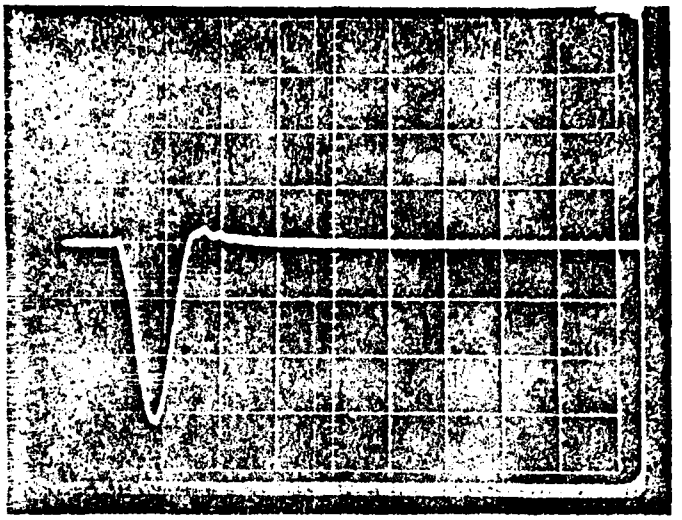

ELECTRICAL INPUT

b.

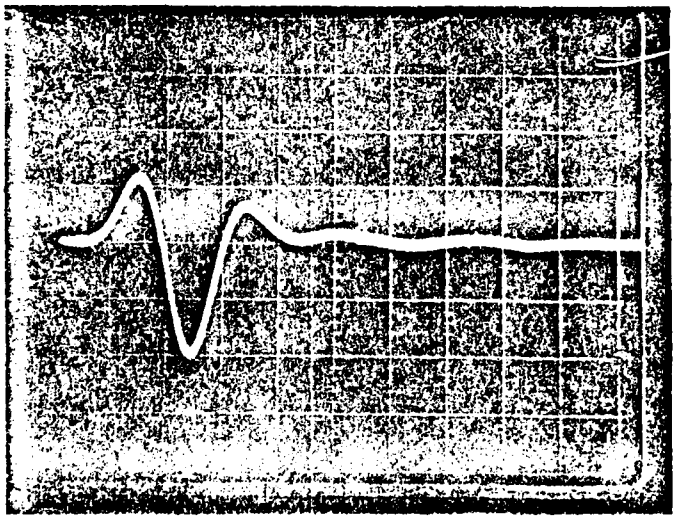

POSFET OUTPUT

→ 0.1 μsec/div

Figure 20. Impulse response of POSFET array element.
a. Electrical drive signal to transmitter.
b. Electrical output signal from POSFET in response to acoustic input.

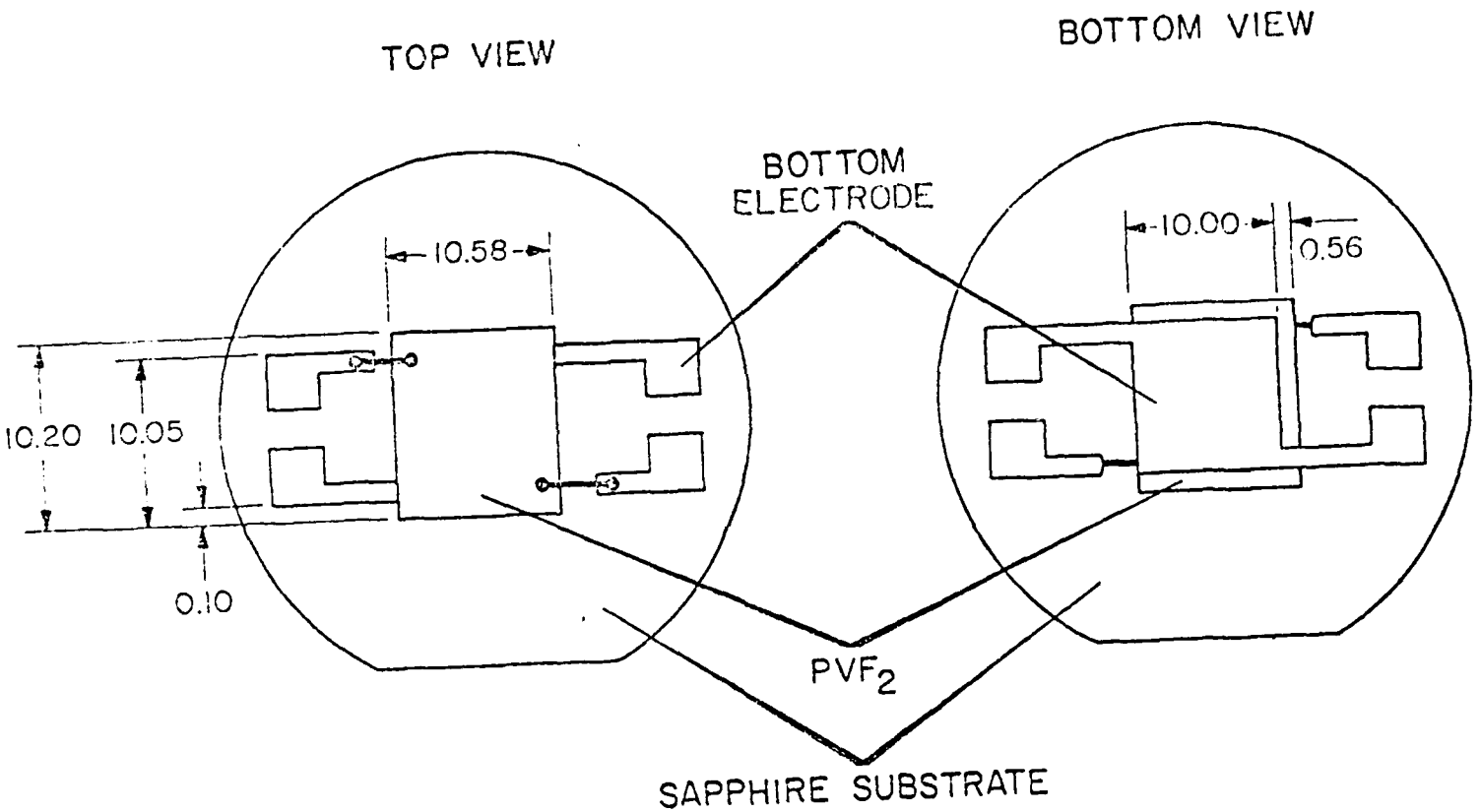

Fig. 21. Geometry of PVF_2 on Sapphire Test Transducers

APPENDIX I

ON THE GENERATION OF HIGH FREQUENCY ACOUSTIC ENERGY WITH POLYVINYLIDENE FLUORIDE*

R.G. Swartz and J.D. Plummer
McCullough Bldg., Rm. 114
Stanford Electronics Laboratories
Stanford, California 94305

Abstract

The polymer piezoelectric polyvinylidene fluoride (PVF_2) has recently shown great promise in medical imaging applications when combined with integrated circuit technology to form a broadband detector of acoustic energy. This paper considers the application of polyvinylidene fluoride as a generator of acoustic energy in the 1 to 10 MHz frequency range. The characteristics of PVF_2 in response to voltage and current-source electrical drive are analyzed and the exceptionally broadband nature of the current drive response is demonstrated. Measured values of the dielectric parameters of PVF_2 are presented and used to calculate the effect on this broadband characteristic of the frequency-varying dielectric constant and high dielectric loss. The multiple-layer stack, a mechanical transformer, is presented and proposed as a method for increasing the available output power from a PVF_2 transducer. Experimental verification of this theoretical modeling is described.

*This work was supported partially under NIH Grant No. 2 P50 GM-17940, and partially under Office of Naval Research Contract No. N00014-78-C-0614.

I. Introduction

The polymer piezoelectric polyvinylidene fluoride (PVF_2) has previously demonstrated unique suitability as a detector of ultrasonic energy in medical imaging applications because of the close acoustic impedance match between it and body tissues. In particular, recent work has demonstrated the viability of monolithic silicon/PVF_2 acoustic sensors [1,2]. An example of this type of transducer structure is shown in Fig. 1. A sheet of PVF_2 is glued to the surface of a silicon wafer. Electrical contact to the PVF_2 is accomplished by means of electrodes evaporated on the PVF_2 and on an SiO_2 layer adjacent to the silicon surface. Diffused within the silicon are the source and drain regions of an MOS transistor, with the lower electrode of the PVF_2 constituting the extended gate of the MOSFET. When an incident longitudinal acoustic wave modulates the thickness of the PVF_2 layer, an electrical signal resulting from piezoelectric action in the transducer appears directly on the gate of the MOS transistor. The MOSFET may then be employed to amplify this signal, or as a multiplexer, to select for further processing one signal from an array of transducer elements.

Simple theory predicts that this piezoelectric/oxide/semiconductor field-effect transistor (POSFET) will display the extremely broadband frequency characteristic plotted in Fig. 2 [1]. This response has been experimentally verified using one and three element test structures. Subsequently, a large array composed of 34 elements, each 0.42 x 9.0 mm, has been constructed. Associated with each array element is an integrated-circuit high frequency amplifier, as seen in the photomicrograph of the silicon surface of the array in Fig. 3. The exceptionally short-duration impulse response of the array sensors (Fig. 4) [2] demonstrates the broadband characteristic made possible by means of PVF_2, which is essential in an imaging transducer. This array is

intended for eventual clinical application in the Stanford ULISYS medical imaging project.

The POSFET receiving transducer technology indicates the great promise of PVF_2. The most functionally-flexible transducer, however, is one that can both transmit and receive. This paper focuses, therefore, on answers to the following questions:

- Can PVF_2 be used to generate high-frequency acoustic energy?
- What are the advantages and best approach to transmitting with PVF_2?

Transmission of acoustic energy with PVF_2 at frequencies above 1 MHz (the range required for medical imaging) has been reported [3-5]. The results obtained from those investigations were generally exploratory in nature, demonstrating the existence and form of an acoustical output. This paper proceeds further, evaluating the potential and means of application of PVF_2, particularly in comparison to the commonly-used ceramic piezoelectric materials.

Inherent acoustic properties of PVF_2 are its broadband response resulting from its acoustic near match to water (the major constituent of body tissues), mechanical flexibility, and wide acceptance angle. The following problems, however, are associated with using PVF_2 as a transmitter.

- Low Dielectric Constant: PVF_2 has a very low dielectric constant in comparison to such materials as lead-zirconate-titanate (PZT). At 2 MHz, for example, the dielectric constant of PVF_2 is approximately 11.5 ε_0 vs 830 ε_0 for PZT-5A. This implies that the input electrical impedance of PVF_2 is very high in comparison to a PZT composite. To generate equal amounts of output acoustic power, therefore, a much higher PVF_2 voltage drive is required.
- High Dielectric Loss: The imaginary component of the complex dielectric constant of PVF_2 is large at frequencies $\geq$500 kHz. Because this loss is responsible for the dissipation of most of the input electric power, only a relatively small fraction appears at the acoustic port. This inherent "insertion loss" cannot be removed by inductive tuning.

- Low k_T: The greatest electromechanical coupling coefficient k_T reported for PVF_2 is 0.205 [6] and, for PZT-5A, it is 0.49 [7]. The square of this number is a measure of the ratio of the transferred electromechanical energy to the total input energy. With equal amounts of available input electrical power, therefore, the PZT transducer will generate greater acoustic output.

These last two problems cannot be resolved with currently available materials although superior polymers, in time, may be developed. The disadvantage of the low dielectric constant can be minimized by the use of multiple layers, discussed in Section IV. In addition, the broadband PVF_2 frequency response may make all of the above characteristics acceptable, depending on particular system applications.

The transducer configuration discussed here is an ideal infinitely high impedance-backed PVF_2 layer. There is little advantage seen in a matched impedance backing, except to raise the resonant frequency, because such a backing would result in excessive power exiting through the rear acoustic port.

II. Transmitting Frequency Response of the PVF_2 Transducer

In a piezoelectric transducer, external tuning of the electrical port is critical for maximizing sensitivity and bandwidth. A series inductor is commonly used to tune out the input capacitance of the transducer at the operating frequency, and the real part of the generator impedance is chosen to match the real transducer impedance [8]. In a low-loss material, however, a small k_T implies a relatively high electrical Q. Inductive tuning of PVF_2 can thus result in a severely reduced bandwidth which is especially undesirable, inasmuch as broadband operation is the principal advantage gained by the use of PVF_2. Initially, therefore, the response of PVF_2 when driven by an untuned, ideal voltage source is analyzed. For simplicity, the dielectric loss is initially neglected, although its effect will be considered in the next section.

If the transducer is modeled by means of the Mason model [9] as shown in Fig. 5, the transfer function becomes

$$\frac{F_{out}}{V_{in}} = \frac{hC_0}{1 - (j\bar{Z}_0/Z_w)\cot\bar{\beta}\ell + (jh^2C_0/\omega Z_w A)} \tag{1}$$

and the output power (plotted vs frequency in Fig. 6) is

$$P_{out} = \frac{|F_{out}|^2}{2Z_w A} \tag{2}$$

where F_{out} is the output force and $Z_w A$ is the acoustic impedance of the water load. The response peaks near the frequency where the thickness of the transducer is one-quarter wavelength. Because this characteristic has a low Q, smooth bandshape, a clean, short-duration impulse response is expected [8].

One measure of the efficiency of a transducer is the insertion loss which is defined to be the ratio of transducer output power to available input power with specified electrical tuning parameters. The lowest insertion loss is normally obtained when the transducer at its resonance is conjugately matched to the source, although this rarely provides the maximum bandwidth. Insertion loss arises as a result of electrical impedance mismatch, dissipative mechanisms within the transducer, output coupling to the rear acoustic port and extraneous modes. Only impedance mismatch and dielectric loss are considered to be of consequence for the rigidly backed PVF_2 transducer.

The output power for a 1 V drive and a 1 cm^2, 100 μm PVF_2 transducer peaks at about [illegible] An inductively-tuned, commercial broadband ceramic transducer of similar dimensions, with no front-matching layers will deliver 60 μW (as calculated for a Panametrics VIP-5-1/2 I transducer with the same drive, based on measured impedance and insertion-loss data) [10]. The output power of a

tuned ceramic transducer with proper front-matching and backing layers, however, can be a factor of 100 greater. Figure 7 plots the calculated two-way insertion loss of PVF_2 as a function of frequency. Figure 7a shows the loss of an untuned transducer, and Fig. 7b illustrates the effect of series inductive tuning. The insertion loss in Fig. 7a is primarily a result of reactive impedance mismatch at the electrical port. As can be seen, tuning improves insertion loss but drastically reduces bandwidth. The one-way insertion loss of the untuned PVF_2 transducer is no better than -20 dB at the quarter-wave resonance; in an optimal ceramic transducer, however, -5 dB or better can be expected, with little reduction in bandwidth.

The response of a PVF_2 transducer driven by a voltage source (Fig. 6) is smooth and broad, but is not as impressive as the frequency response of the PVF_2-POSFET receiver (Fig. 2) that extends ideally to dc. The condition required for this response is that the transducer's electrical port be capacitively loaded, a constraint satisfied by the MOSFET gate in Fig. 1. The equivalent mode of operation for a transmitting PVF_2 structure is obtained when the transducer is driven by a current source. When the Mason model of Fig. 5 is modified accordingly, the transfer relationship can be derived as

$$\frac{F_{out}}{I_{in}} = \frac{h}{j\omega} \frac{1}{1 - (j\bar{Z}_0/Z_w) \cot \bar{\beta}\ell} \tag{3}$$

which leads to a transmit frequency characteristic of the form of Fig. 2. The calculated acoustic output power (plotted in Fig. 8)

$$P_{out} = \frac{|I_{in}|^2 R_a}{2} \tag{4}$$

is also nearly constant. The equivalent circuit of Fig. 9, derived from the Mason model of Fig. 5, represents the PVF_2 transducer below resonance. The principal components are the clamped capacitance, C_0; the dielectric loss resistance, R_f; and the radiation resistance R_a, representing actual acoustic output power. The broadband nature of the response under current drive can be understood by recognizing that, ignoring dielectric loss, the radiation resistance R_a of PVF_2 operated in the quarter-wave mode is virtually constant down to dc. Because of the rigid acoustic backing, any electric-field-induced strain must appear as displacement of the front surface of the transducer.

The current-source-driven mode of operation of PVF_2 has the following advantages:

- The overall impulse response is better than for other electrical drive methods because the frequency response extends over a broader range.
- The phase of the transfer characteristic will vary linearly below the resonant frequency, a necessary requirement for distortion-free transmission [11].
- Extension of the response to frequencies far below resonance indicates that a single PVF_2 transducer could be used over a wide range of operating frequencies.

Although an "ideal" current source cannot be obtained at all frequencies, the requirement for broadband operation of this type is merely that the current-source output impedance must be much higher than the electrical input impedance of the transducer. This method is impractical at low frequencies because there the essentially capacitive transducer impedance becomes very large, thus requiring the current source to stand-off an excessive voltage.

III. Effect of Dielectric Loss

Dielectric loss has been neglected in the above calculations, which is a reasonable procedure for typical ceramic transducers. The high k_T of these

piezoelectrics makes acoustic loading rather than dielectric loss a dominant factor in the electrical Q. As a consequence, most electrical power is coupled to the acoustic ports, and relatively little is lost in the ceramic dielectric.

Other researchers [12], however, have reported the high dielectric loss in PVF_2. Figure 12 plots the measured dielectric constant and loss tangent of a 30 μm sample of uniaxially stretched and poled Kureha PVF_2 film. These curves were obtained by measuring the electrical input impedance of an acoustically unloaded film sufficiently below the half-wave resonant frequency so that

$$Y_{in} = j\omega C_0 \left(1 + \frac{e_{33}^2}{c_{33}^E \varepsilon_{33}^S}\right) \qquad (5)$$

which for PVF_2 (where $e_{33}^2/c_{33}^E\varepsilon_{33}^S \ll 1$), becomes

$$Y_{in} \approx j\omega C_0 = j\omega \frac{A}{\ell}(\varepsilon' - j\varepsilon'') = \frac{j\omega A\varepsilon'}{\ell}(1 - j\tan\delta_E) \qquad (6)$$

where ε' and ε'' are the real and imaginary parts of the complex dielectric constant and $\varepsilon''/\varepsilon' \triangleq \tan\delta_E$, the dielectric loss tangent [13].

Earlier calculations of the electromechanical transfer relationships and frequency response have assumed a uniform dielectric constant. It is not difficult to include the variation of ε with frequency within the standard Mason model; however, the dependence of the elastic and piezoelectric factors on frequency should be determined as well. Such parameters have been measured as a function of temperature for PVF_2 [6], but there is an absence of knowledge of their variation with frequency. Although frequency-independent elastic and piezoelectric constants are assumed in the calculations to follow, the variation of the dielectric constant is included.

A property of a PVF_2 transducer operating in the $\lambda/4$ mode is that, in the absence of dielectric or mechanical loss, conservation of energy requires that the real electric input power must equal the output acoustic power, inasmuch as very little energy is coupled into the back acoustic port. In the presence of dielectric loss, however, this is no longer true. When tan δ_E is nonzero, the power dissipated in the loss resistance R_f (see Fig. 9) can greatly exceed that acoustically radiated. Figure 11 is a plot of the calculated acoustic output and electrical input power as a function of frequency for a 30 μm PVF_2 transducer under current-source drive; the measured variations of the dielectric constant and dielectric loss have been included. The curves were obtained from the Mason model in Fig. 5. It can be seen that the impressive broadband acoustic output response is relatively unaffected by dielectric loss; however, the discrepancy between the real input and output power indicates that most electrical power is dissipated within the body of the transducer. This has the following important implications:

- The transducer will be internally heated by this dielectric dissipation. Internal heating may eventually raise the temperature to the point where the PVF_2 material is depoled. The maximum duty cycle for transducer operation will depend, therefore, on the peak power used for transmitting and on the thermal conductivity of the various components of the transducer structure.

- The dielectric-loss component cannot be tuned inductively. The insertion loss plotted in Fig. 7b where δ_E has been neglected reaches a satisfactory minimum at the tuned frequency. Actually, however, even with tuning, most of the electrical input power is dissipated. This constitutes an inherent minimum insertion loss regardless of the electrical-drive method employed. As can be seen in Fig. 11, this loss is minimum at the quarter-wave frequency (for the 30 μm PVF_2) it is approximately -17 dB (two-way).

Fig. 12 plots the calculated input electrical and output acoustic power vs frequency for current-source-driven PVF_2 which has been inductively parallel

tuned In Fig. 12a, the transducer has been tuned below its resonant frequency. Its "inherent" untunable two-way insertion loss is approximately -30 dB which compares poorly to well-designed modern ceramic transducers, and its frequency response has deteriorated substantially.

Figure 12b is the predicted response of a PVF_2 transducer inductively tuned very near the resonant frequency. The minimum two-way insertion loss remains approximately -19 dB, but the bandshape is more uniform which implies a cleaner impulse response. A transmitting transducer tuned at resonance may be an acceptable alternative to a ceramic transducer in applications where other features of PVF_2 prove advantageous.

Before proceeding with experimental verification of some of the predicted results in this section, we turn to an alternative technique for improving the overall transmit efficiency of the simple PVF_2 structure.

IV. Multiple Layers

As discussed in Section I, the low dielectric constant of PVF_2 relative to that of ceramic piezoelectric materials can present a problem in transmitting applications. For example, using a 100 V signal generator, it is possible to generate an acoustic output intensity of 20 W/cm^2 at 5 MHz in an electrically tuned, efficient ceramic transducer. It can be shown from the data in Figs. 10 and 11 that because of its lower dielectric constant, the generation of a comparable acoustic output intensity would require an 800 V signal in a PVF_2 transducer $\lambda/4$ resonant at 5 MHz [9].

Lin[illegible] [14] has proposed a method for increasing the power output from a voltage-source-driven transducer, however, by using a multiple-layer stack of PVF_2 (Fig. 13). The transducer is backed by a high acoustic impedance,

and the materials of the alternating layers have reversed polarity. The following features of this scheme can be understood by recognizing that the layers are electrically in parallel and acoustically in series:

- The transducer is resonant at a frequency where the total stack thickness is one-quarter wavelength.
- For a constant total stack thickness and voltage-source input, the acoustic output power increases as the square of the number N of layers within the stack; that is,

$$P_{out} \propto N^2 \tag{7}$$

For a transducer thickness of 100 μm, the calculated output power vs frequency is plotted in Fig. 14 for various numbers of layers (dielectric loss has been again neglected). The thickness of each layer is 100 μm/N. Observe that for a constant source voltage V, the total electric-field-induced strain across the stack is the result of an effective series voltage of NV. The output power is thus proportional to the square of NV, which leads to the relationship expressed in Eq. (7). The use of a multiple-layer stack may be considered an approach to lowering the electrical input impedance.

This technique based on multiple layers has another interesting aspect, as exemplified in Fig. 15. Here, the thickness of the individual layer has been held constant while the number of layers is changed so that the total stack thickness varies. It can be observed in the figure that peak power and Q remain constant and that the resonant frequency is shifted. As before, the resonant frequency depends on the total thickness of the stack,

$$\omega_0 \propto \frac{1}{N\ell} \tag{8}$$

where ℓ is the layer thickness and N is the number of layers. The electrical

input impedance at resonance is determined, to first order, by the clamped capacitive impedance of the N layers which are electrically in parallel,

$$Z_{in} \simeq \frac{1}{N\omega_0 C_0} \propto \frac{1}{N\omega_0 / \ell} \tag{9}$$

The output power is proportional to the reciprocal of the impedance,

$$P_{out} \propto \frac{V^2}{Z_{in}} \tag{10}$$

which, when combined with Eqs. (8) and (9) yields

$$P_{out} \propto \frac{1}{\ell^2} \tag{11}$$

Therefore, the output power at resonance does not depend on the number of layers in the stack but only on the thickness of the individual layer. To build a PVF_2 transducer that delivers maximum output acoustic power from a voltage-source drive, the minimum layer thickness available should be selected and then these layers stacked until the composite is quarter-wave resonant at the desired operating frequency.

Although this scheme can optimize the transmitter, it does not improve the same transducer used as a receiver. Because alternating layers are 180° out of phase, the acoustically generated electrical signals received from these transducers will cancel. An electrical signal can be properly detected only if there are an odd number of layers, and then it would be of the same magnitude as that from a single thin layer.

This multiple-layer arrangement can be of use in a current-source-driven PVF_2 transducer as well. A problem with current-source drive is that the stand-off voltage requirement for the current source may exceed the voltage

capability of the driver. This maximum driver voltage V_{max} limits the available driver current and, therefore, the maximum output power:

$$P_{max} \propto V_{max}^2 \tag{12}$$

If a current source is substituted for the voltage source in the multiple-layer transducer of Fig. 13, and then its output is increased until V_{max} appears at the electrical terminals, the multilayered current-source conditions become identical to those of the voltage-drive case; V_{max} appears across each layer, and the total series voltage across the stack is then NV_{max}. The new P_{max} is

$$P'_{max} \propto N^2 V_{max}^2 \propto N^2 P_{max} \tag{13}$$

By reducing the electrical input impedance, the maximum input current can be increased substantially before the voltage limitation is again reached.

If the total thickness of the multiple layer PVF_2 stack is T, a transmitting transducer can be modeled mechanically as a single transducer of thickness T. Electrically, it can be modeled as in Fig. 16 where the transducer symbol denotes a transducer of thickness T and the transformer turns ratio N is the number of layers in the stack such that $T = N\ell$.

Because stacking performs essentially the function of an electrical transformer, one might assume that a conventional transformer would perform as well and with considerably less fabrication difficulty. There are some cases, however, when multiple layers are desirable, such as when operation is required at a frequency below the resonance of the available material. It can be seen in Fig. 11 that maximum efficiency is achieved when operating at the resonant frequency; several layers can be stacked to produce peak operation.

Figure 17 illustrates a scheme for fabricating a monolithic linear array of transmitting transducers. The electrode on one face of the PVF_2 is masked and etched to form vertical strips. A ground electrode is deposited on the back. The PVF_2 is then folded horizontally in accordion fashion to realize an M+1 layer transducer array of K elements, where M is the number of folds and K is the number of vertical electrode strips.

V. Monolithic Silicon/PVF_2 Transmitting Structures

Although the method in Fig. 17 should be sufficient to construct a transmitting-transducer array with conventional connections and multiplexing technology, it may be desirable to utilize the monolithic integrated-circuit/transducer approach. One method for the construction of a monolithic single-layer array is illustrated and electrically modeled in Fig. 18. The array could contain several basic cells, each with transmit and receive MOS transistors which are capacitively coupled to the PVF_2 transducer via the intervening glue and SiO_2 layers, similar to the POSFET device of Fig. 1. The transmit transducer is used as a multiplexer for the drive signal or as a component of the current-drive circuitry. For either application, it can be designed to act like a high-impedance load during the receive mode of operation. In this configuration, the maximum transmit voltage is limited by the breakdown voltage of the MOS transistors. Multiple layers may circumvent this limitation; however, if very small transducer elements are required, the technically difficult problem of aligning the PVF_2 electrode (Fig. 18) with the coupling electrodes on the silicon surface may render a monolithic multiple-layer array impractical.

VI. Experimental Measurements

Experimental verification was attempted of the theoretical results described in Sections II and III. For these measurements, a 1.6 cm^2 brass-

rod backed PVF_2 transducer was used as an acoustic wave generator, and the PVF_2-POSFET array elements described in Section I were employed as receivers. An approximation of a matched voltage-source driver was obtained by use of the 50 Ω output port of a standard function generator. Additionally, a current driver capable of sourcing 180 mA and standing off 20 V in a linear mode of operation was constructed [15].

Initially, the brass rod-backed transducer was used as both a transmitter and receiver. It was positioned in a water tank opposite a brass block and electrically driven first with a voltage and then with a current "impulse". These impulses were actually pulses sufficiently narrow so that, if the pulsewidth was further reduced, only the amplitude (not the shape) of the response changed. The echo from the brass block, as received by the transducer, is shown in Fig. 19 under both voltage and current drive. Although the voltage-driven PVF_2 response in Fig. 19a decays quite rapidly, the current-driven impulse response in Fig. 19b is even closer to ideal.

Using a transient analysis based on the assumption of transducer-edge excitation [16], it has been predicted [17] that the ideal one-way response of a quarter-wave resonant transducer acoustically matched at the front interface is close to a single-cycle stress wave at the resonant frequency of the transducer. A means of determining the ideal two-way response is derived in Fig. 20 by assuming that the ideal single-cycle strain echo has returned from a reflector to the generating transducer. The transducer is again assumed to be acoustically matched to the medium so that there is no reflection at the front interface. Figure 20a plots this strain wave at various times as it propagates across the thickness of the transducer. A zero strain condition exists at the back face of the transducer because it is rigidly clamped by the high-impedance load and, as a result, the reflected strain wave will have opposite sign.

This strain directly induces a similar electric-field distribution via piezoelectric action. The total voltage across the transducer at any given time can be determined by integrating this spatial field distribution over the thickness. This can be visualized graphically by calculating the total area under the curves in Fig. 20a to obtain the plot in Fig. 20b. Comparison reveals a close resemblance of Fig. 20b to the measured impulse response of the current-driven PVF_2 transducer in Fig. 19b. The differences are a slight additional ringing in the PVF_2 two-way output and a central positive peak that is too large relative to the negative peaks. These are thought to originate from the slight acoustic impedance mismatch at the front surface.

An element of the POSFET linear array (Fig. 3) was then selected as a receiving transducer, and the two-way frequency response was measured by again using the current driver. The result is plotted in Fig. 21. Here, it can be seen that the two-way response appears to flatten out below 5 MHz and reaches an apparently stable level at the lower frequency limit of the current driver. Comparison of this response to the curves in Fig. 10 indicates that the agreement between the measured result and theory is promising.

An experiment was performed to determine the effect of inductive tuning on a current-source driven PVF_2 transducer. Again, the 1.6 cm^2 brass-rod backed PVF_2 transducer was the transmitter and a PVF_2 array element was the receiver. Parallel inductors tuned the transmitter at various frequencies, and the received signal was measured both with and without tuning. It was seen that the gain in output amplitude with tuning is inversely related to frequency. This was predicted by the theoretical plots in Fig. 12 where the output power gain factor from tuning is 10:1 below resonance but only 6:1 at resonance. The price paid for this increase in output level is the long ring-down of the response (Fig. 22).

VII. Conclusions

This paper has investigated various ways of using PVF_2 as a transmitting transducer. It was found that, in addition to standard electrical-drive techniques, current drive has impressive advantages. One is the attainment of perhaps the best two-way impulse response ever obtained by a piezoelectric medical-imaging transducer, and another is the possibility of fabricating a single transducer that can operate with linear phase variation, at frequencies below its resonance. Experimental measurements of transmit efficiency and frequency response have confirmed the basic modeling results described in this paper.

In some ways, PVF_2 has proved inferior to ceramic piezoelectrics because of the low k_T and dielectric constants. Consequences of these weaknesses can be minimized by use of multiple-layer structures. Such problems as the inherent untunable insertion loss caused by dielectric loss cannot be presently resolved. Eventual improvements in its piezoelectric parameters and reduction of its dielectric loss may ultimately cause PVF_2 to become the transducer material of choice in medical imaging applications.

VIII. Acknowledgments

The authors wish to acknowledge the support of J.D. Meindl in the completion of this study. The contribution of J.G. Linvill, described in this paper, is deeply appreciated. The assistance of P. Jerabek and J.T. Walker in the design of the transducers, test fixtures, and electronics has been most helpful. Finally we acknowledge the many discussions with R.W. Timme which were very useful inputs for this work.

IX. References

1. R.G. Swartz and J.D. Plummer, "Monolithic Silicon-PVF_2 Piezoelectric Arrays for Ultrasonic Imaging," in Acoustical Holography, Vol. 8 (A. Metherell, ed.), Plenum Press, New York, 1979.

2. R.G. Swartz and J.D. Plummer, "Integrated Silicon-PVF_2 Acoustic Transducer Arrays," to be published IEEE Trans. on Electron Devices, Nov. 1979.

3. H. Sussner, D. Michas, A. Assfalg, S. Hunklinger, and K. Dransfeld, "Piezoelectric Effect in Polyvinylidene Fluoride at High Frequencies," Phys. Letts., 45A, 5 Nov 1973, pp. 574-476.

4. L.N. Bui, H.J. Shaw, and L.T. Zitelli, "Study of Acoustic Wave Resonance in Piezoelectric PVF_2 Film," IEEE Trans. on Sonics and Ultrasonics, SU-24, Sep 1977, pp. 331-336.

5. N. Chubachi and T. Sannomiya, "Composite Resonator Using PVF_2 Film and Its Application to Concave Transducer for Focusing Radiation of VHF Ultrasonic Waves," 1977 Ultrasonic Symp. Proc., pp. 119-123.

6. H. Ohigashi, "Electromechanical Properties of Polarized Polyvinylidene Fluoride Films as Studied by the Piezoelectric Resonance Method," J. Appl. Phys., 47, Mar 1976, pp. 949-955.

7. H. Jaffe and D.A. Berlincourt, "Piezoelectric Transducer Materials," Proc. IEEE, 53, Oct 1965, pp. 1372-1386.

8. C.S. DeSilets, Transducer Arrays Suitable for Acoustic Imaging, Ph.D. dissertation, Ginzton Laboratory Report No. 2833, Stanford University, Jun 1978, Chapter 2.

9. D. Berlincourt, "Piezoelectric Crystals and Ceramics," in Ultrasonic Transducer Materials (O.E. Mattiat, ed.), Plenum Press, New York, 1971, pp. 72-79.

10. R.G. Swartz, Application of Polyvinylidene Fluoride to Monolithic Silicon/PVF_2 Transducer Arrays, Ph.D. dissertation, Stanford Electronics Laboratory Report No. 79-013, Stanford University, May 1979, Chapter 7.

11. P.F. Panter, Modulation, Noise and Spectral Analysis Applied to Information Transmission, McGraw-Hill Book Co., New York, 1965, pp. 68-71.

12. H. Sussner, D.E. Horne, and D.Y. Yoon, "A New Method for Determining the Pyroelectric Coefficient of Thin Polymer Films Using Dielectric Heating," Technical Report of IBM Research Laboratory, San Jose, Calif.

13. C.E. [illegible], G.W. Smith, and C.R. Westgate, "The Dependence of the Small-Signal Parameters of Ferroelectric Ceramic Resonators upon State of Polarization," IEEE Trans. on Sonics and Ultrasonics, SU-11, Jun 1964, pp. 6-13.

14. J.G. Linvill, PVF2 - Models, Measurements, Device Ideas, TR No. 4834-3, Stanford Electronics Laboratories, Stanford University, Stanford, Calif., Mar 1978, pp. 83-88.

15. J.T. Walker, private communication.

16. E.G. Cook, "Transient and Steady-state Response of Ultrasonic Piezoelectric Transducers," 1956 IRE Convention Records, 4, pp. 61-69.

17. L. Bui, H.J. Shaw, and L.T. Zitelli, "Experimental Broadband Ultrasonic Transducers Using PVF2 Piezoelectric Film," Electronics Letts., 12, 1976, p. 393.

X. Figure Captions

Fig. 1. PVF_2-MOSFET TRANSDUCER

Fig. 2. OUTPUT-VOLTAGE/INPUT-STRESS TRANSFER RELATIONSHIP FOR THE λ/4 RESONANT PVF_2 TRANSDUCER.

Fig. 3. [illegible]-TOMICROGRAPH OF 34 ELEMENT POSFET ARRAY.

Fig. 4. IMPULSE RESPONSE OF A POSFET ARRAY ELEMENT.

Fig. 5. MASON-MODEL EQUIVALENT CIRCUIT FOR THE VOLTAGE-DRIVEN PVF_2 TRANSDUCER.

Fig. 6. OUTPUT POWER VS FREQUENCY FOR A VOLTAGE-SOURCE DRIVE, 100 μm PVF_2 TRANSDUCER.

Fig. 7. TWO-WAY INSERTION LOSS AS A FUNCTION OF FREQUENCY.
a. Untuned PVF_2 transducer.
b. Inductively tuned transducer.

Fig. 8. OUTPUT POWER VS FREQUENCY FOR A CURRENT-DRIVEN PVF_2 TRANSDUCER, 1A DRIVE.

Fig. 9. PVF_2 EQUIVALENT CIRCUIT BELOW λ/4 RESONANCE.

Fig. 10. DIELECTRIC PARAMETERS OF POLYVINYLIDENE FLUORIDE VS FREQUENCY.
a. Dielectric constant for PVF_2.
b. Dielectric loss tangent ($\tan \delta_E$) for PVF_2.

Fig. 11. ELECTRICAL INPUT AND ACOUSTIC OUTPUT POWER OF PVF_2 UNDER 1A CURRENT DRIVE IN THE PRESENT OF DIELECTRIC LOSS.

Fig. 12. PVF_2 ELECTRICAL INPUT AND ACOUSTIC OUTPUT POWER FOR A 1A CURRENT DRIVE.
a. With parallel tuning below resonance.
b. With tuning at resonance.

Fig. 13. MULTIPLE-LAYER TRANSMITTER.

Fig. 14. NUMBER OF PVF_2 LAYERS VS OUTPUT POWER.

Fig. 15. NUMBER OF PVF_2 LAYERS VS RESONANT FREQUENCY.

Fig. 16. ELECTRICAL MODEL OF A CONSTANT-THICKNESS PVF_2 TRANSDUCER COMPOSED OF LAYERS ELECTRICALLY IN PARALLEL.

Fig. [illegible] [illegible]TIPLE-LAYER PVF_2 FABRICATION SCHEME.

Fig. [illegible] [illegible]SMIT/RECEIVE INTEGRATED MONOLITHIC TRANSDUCER.
a. Cross section.
b. Electrical equivalent circuit.

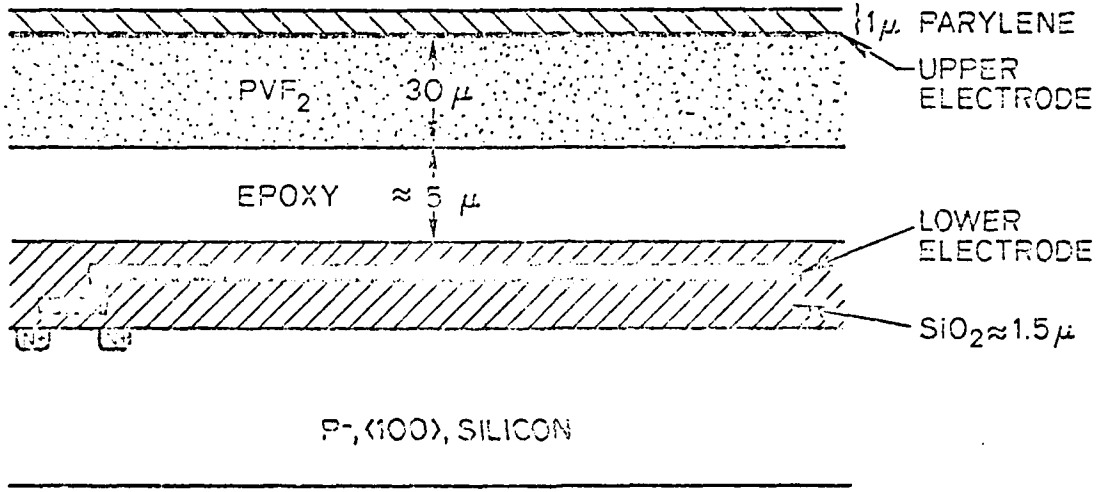

FIG. 1 PVF_2 -MOFSET TRANSDUCER

A21

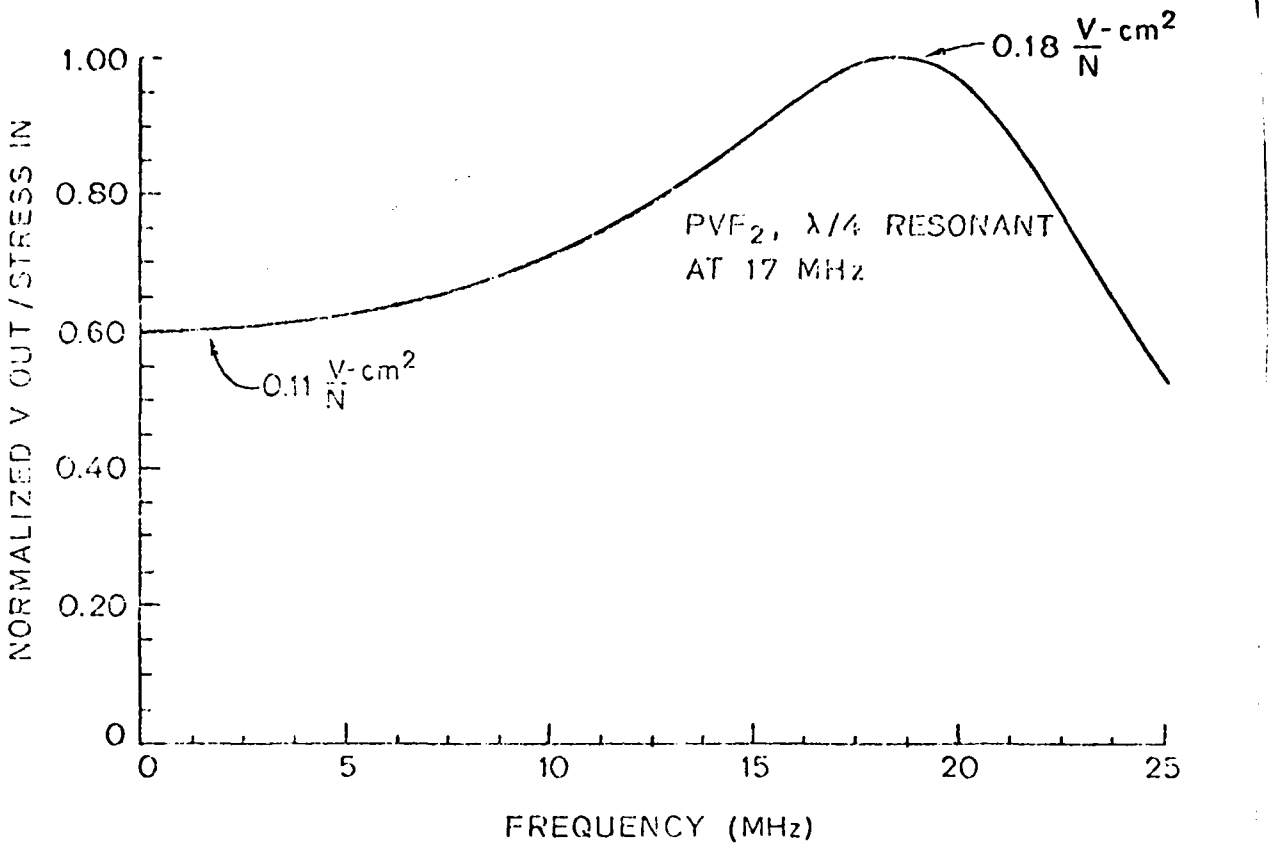

FIG. 2 a.

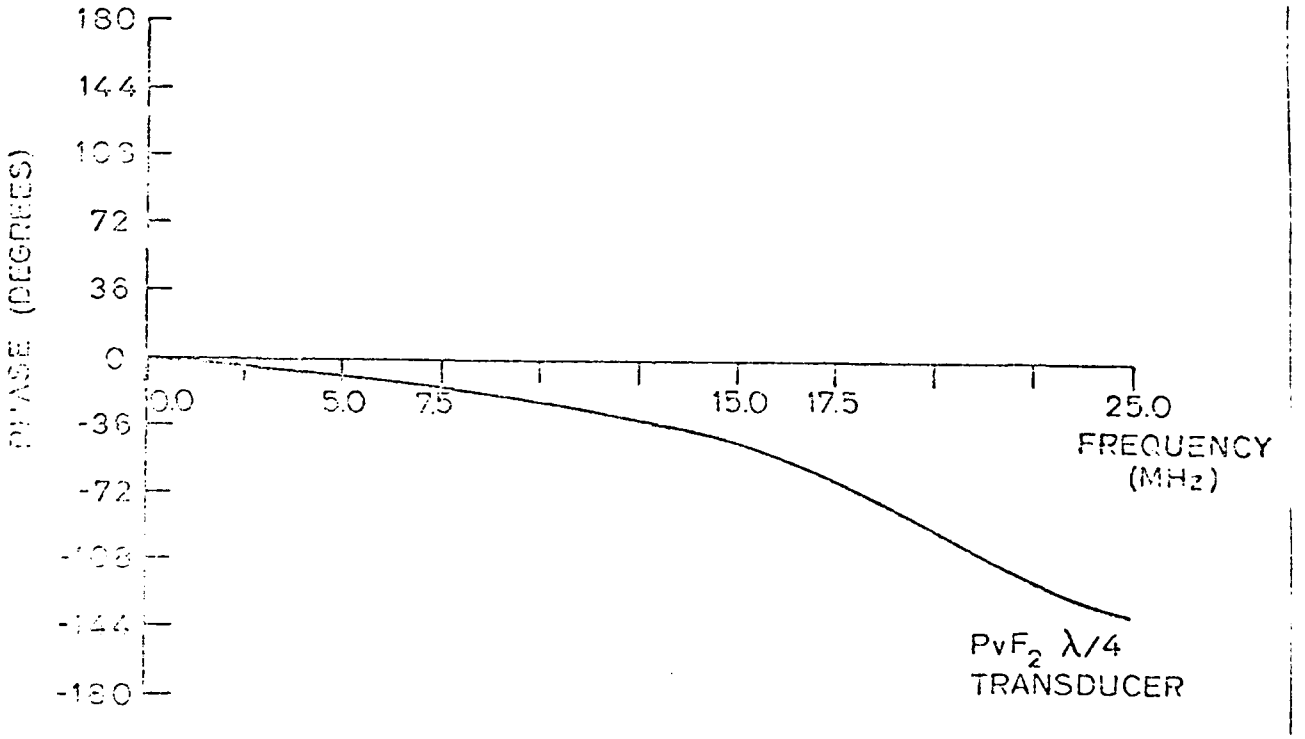

FIG. 2 b.
OUTPUT-VOLTAGE/INPUT-STRESS TRANSFER RELATIONSHIP FOR THE λ/4 RESONANT PVF_2 TRANSDUCER

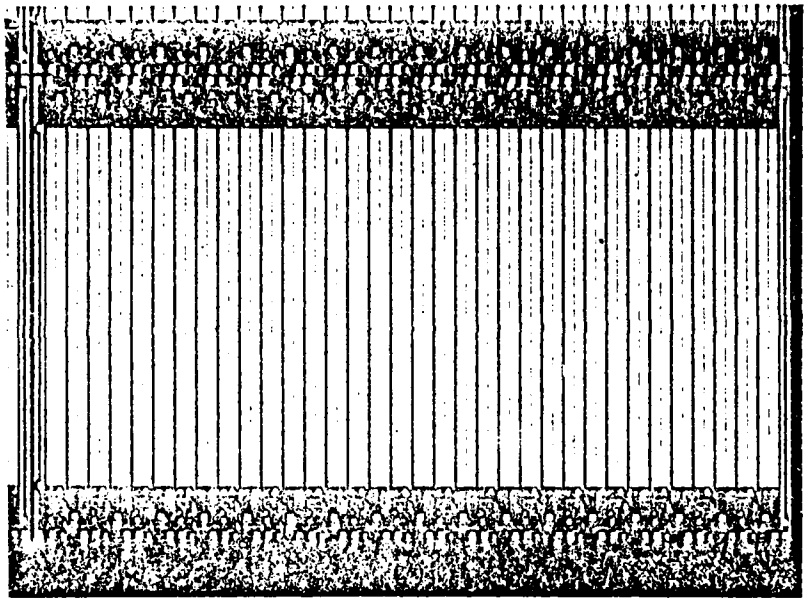

FIG. 3 PHOTOMICROGRAPH OF 34 ELEMENT POSFET ARRAY

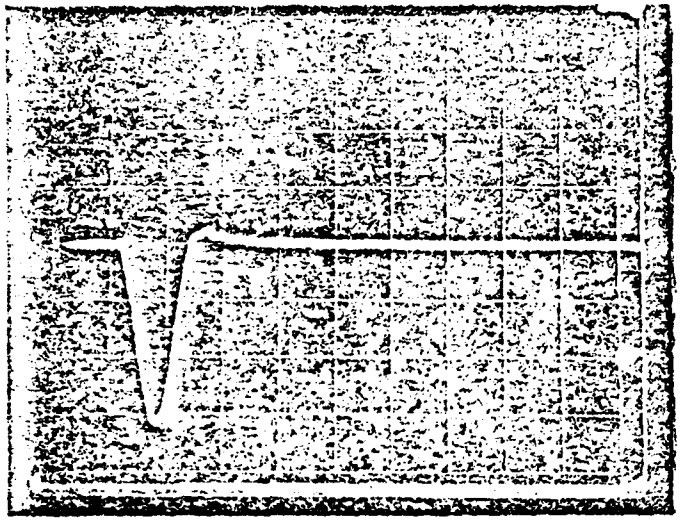

ELECTRICAL INPUT

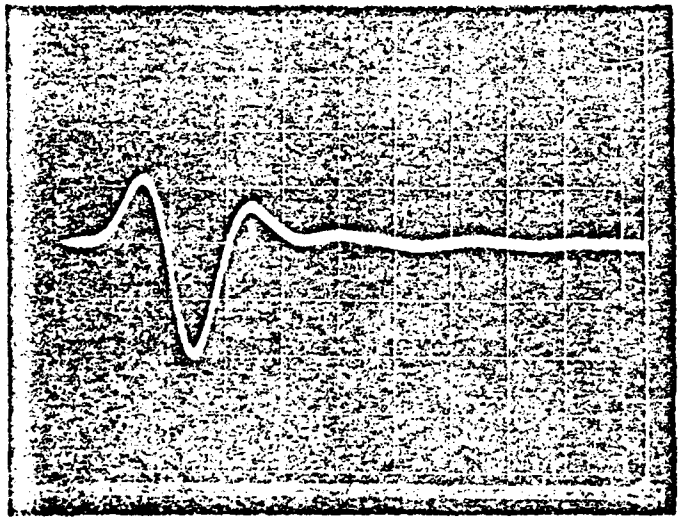

POSFET-3 OUTPUT

→ 0.1 μsec/div

FIG. 4 IMPULSE RESPONSE OF A POSFET ARRAY ELEMENT

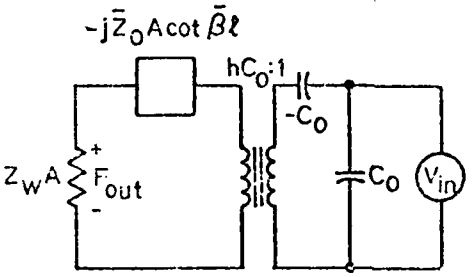

FIG. 5 MASON-MODEL EQUIVALENT CIRCUIT FOR THE VOLTAGE-DRIVEN PVF_2 TRANSDUCER.

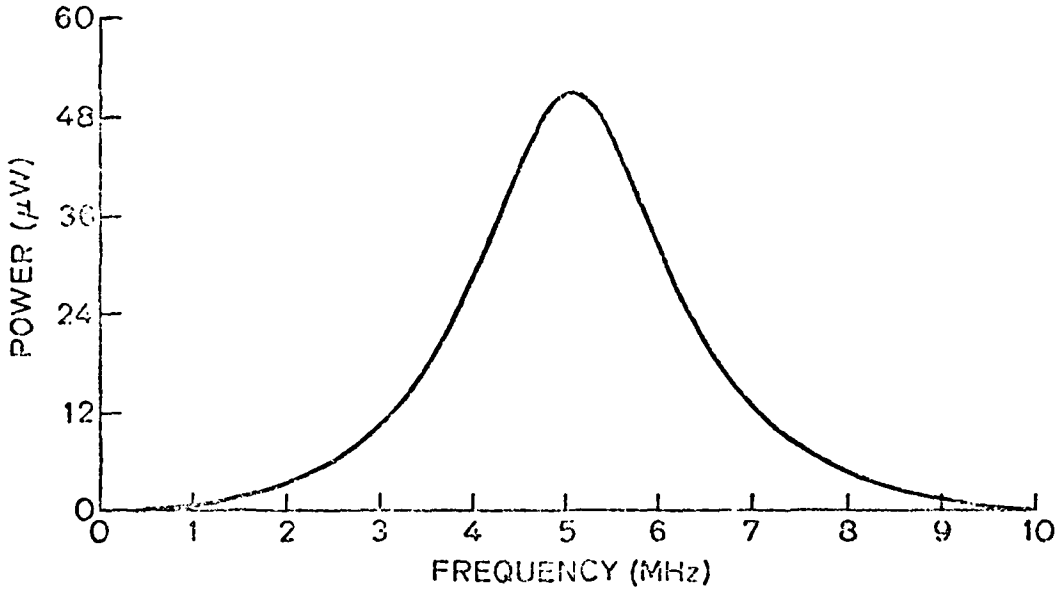

FIG. 6 OUTPUT POWER VS FREQUENCY FOR A VOLTAGE-SOURCE DRIVE, 100 μm PVF_2 TRANSDUCER

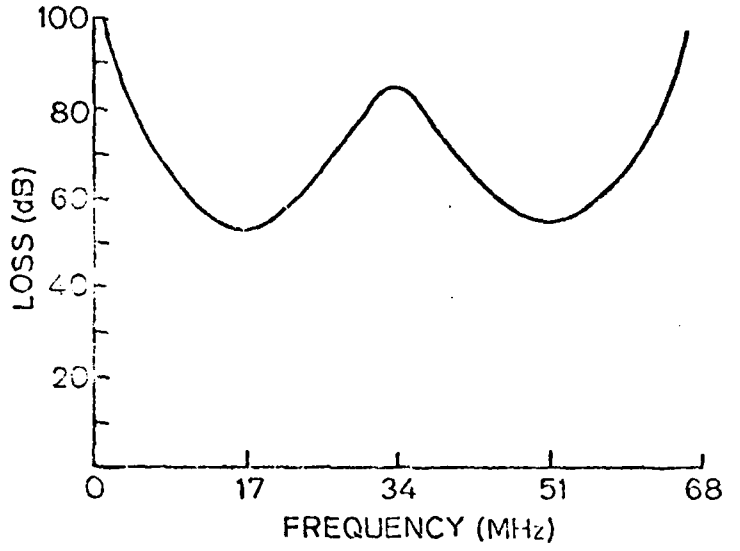

A. Untuned PVF_2 transducer

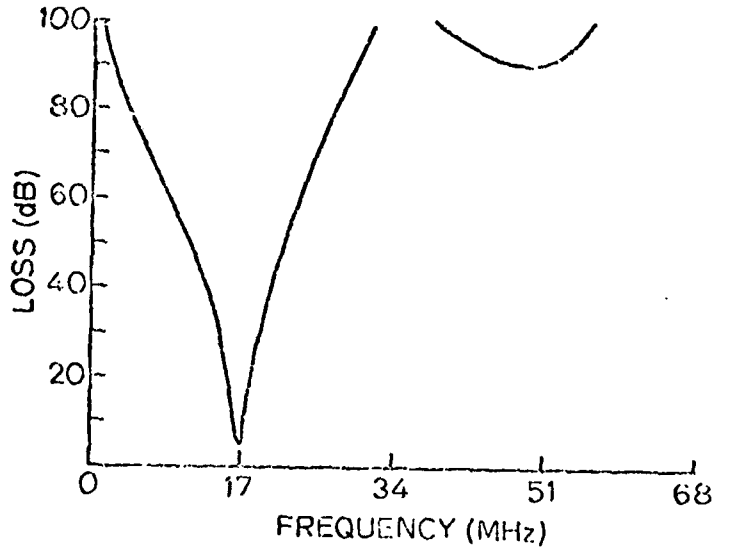

B. Inductively tuned transducer

FIG. 7 TYPICAL INSERTION LOSS AS A FUNCTION OF FREQUENCY

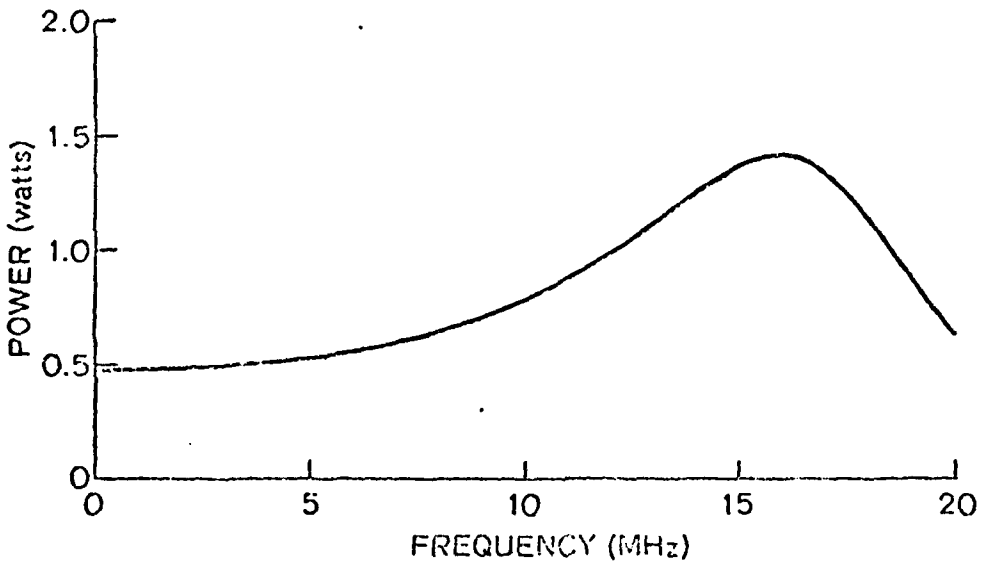

FIG. 8 OUTPUT POWER VS FREQUENCY FOR A CURRENT-DRIVEN PVF_2 TRANSDUCER, 1A DRIVE

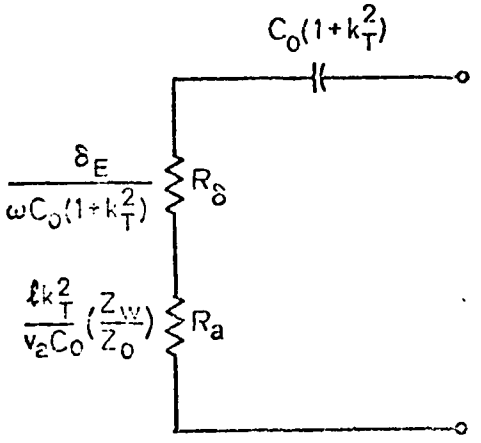

FIG. 9 PVF_2 EQUIVALENT CIRCUIT BELOW $\lambda/4$ RESONANCE

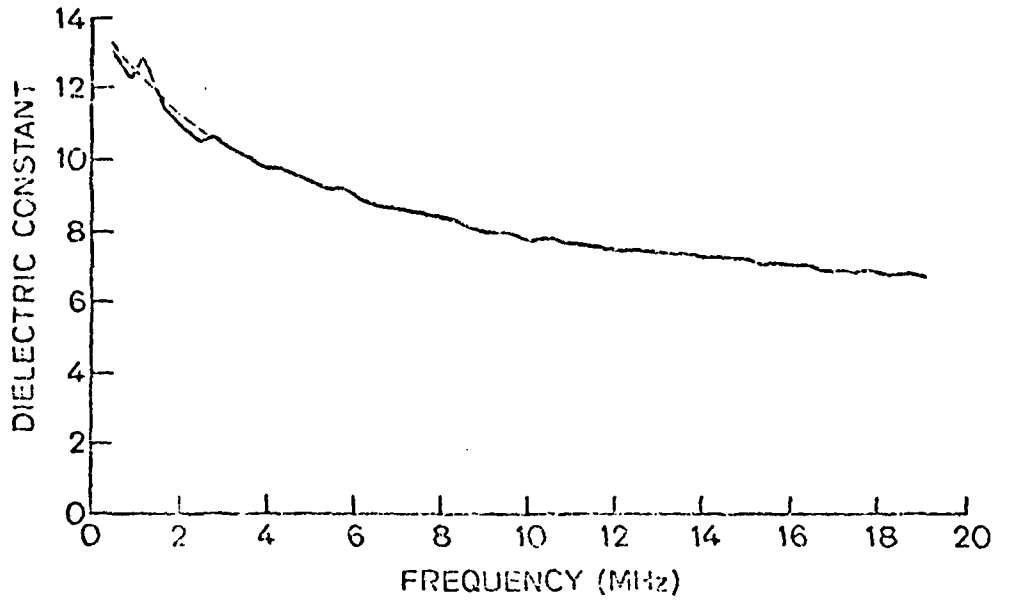

A. Dielectric constant for PVF_2

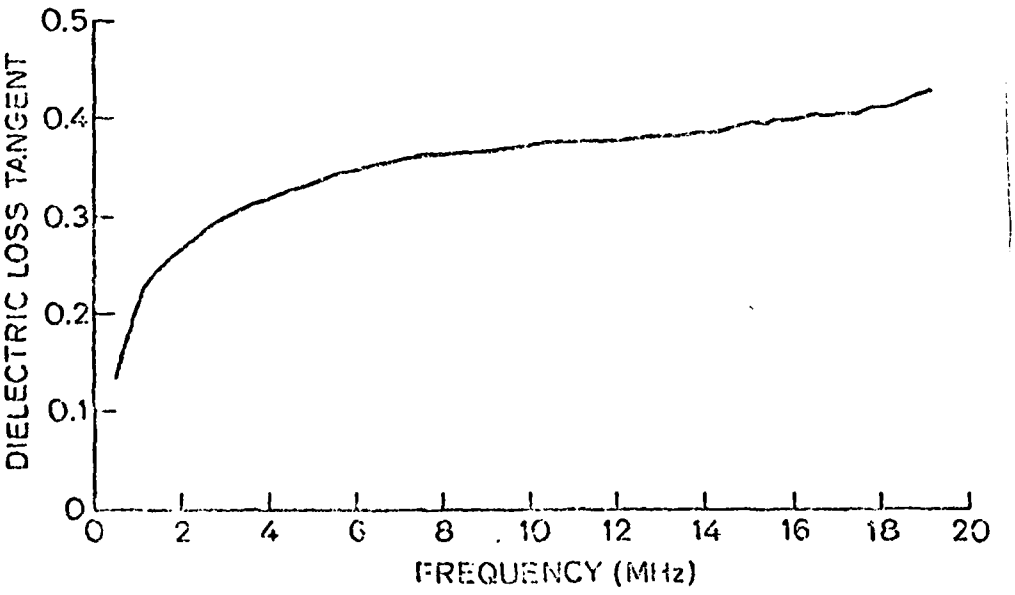

FIG. 10 DIELECTRIC PARAMETERS OF POLYVINYLIDENE FLUORIDE VS FREQUENCY

B. Dielectric loss tangent (tan δ_E) for PVF_2.

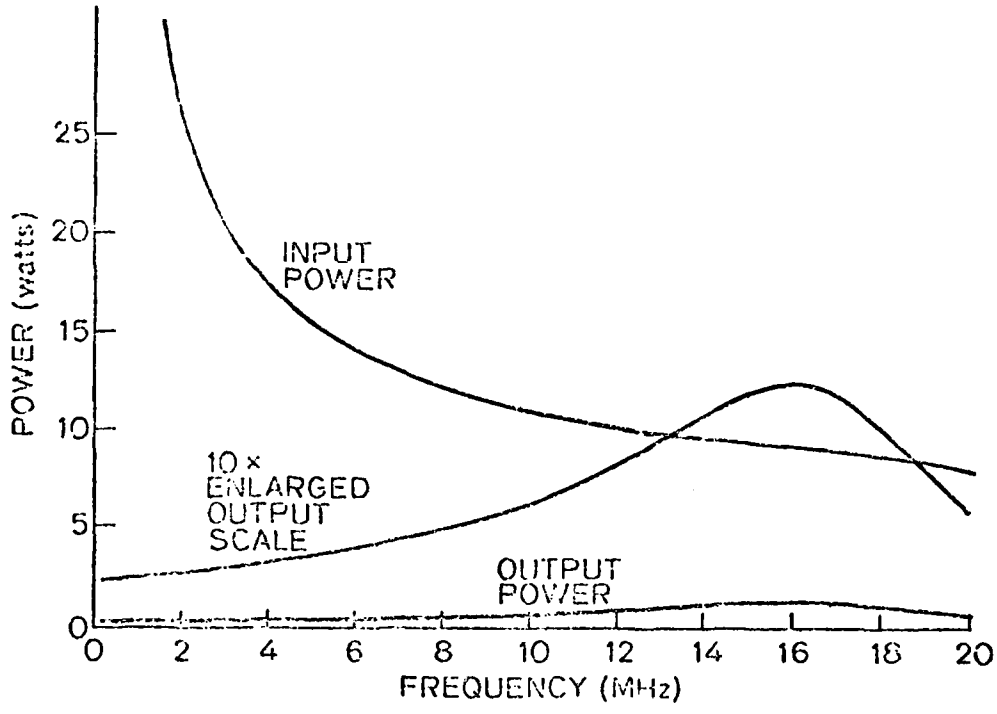

FIG. 11 ELECTRICAL INPUT AND ACOUSTIC OUTPUT POWER OF PVF_2 UNDER 1A CURRENT DRIVE IN THE PRESENT OF DIELECTRIC LOSS

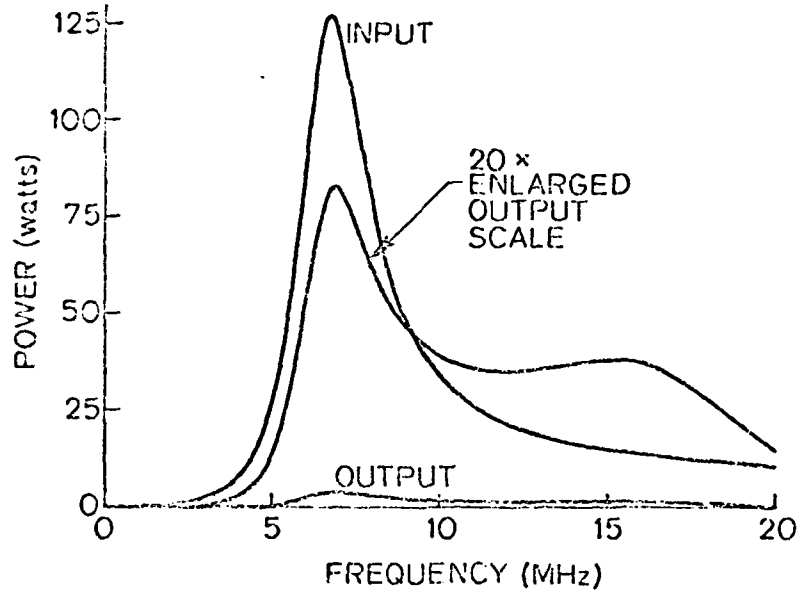

a. With parallel tuning below resonance

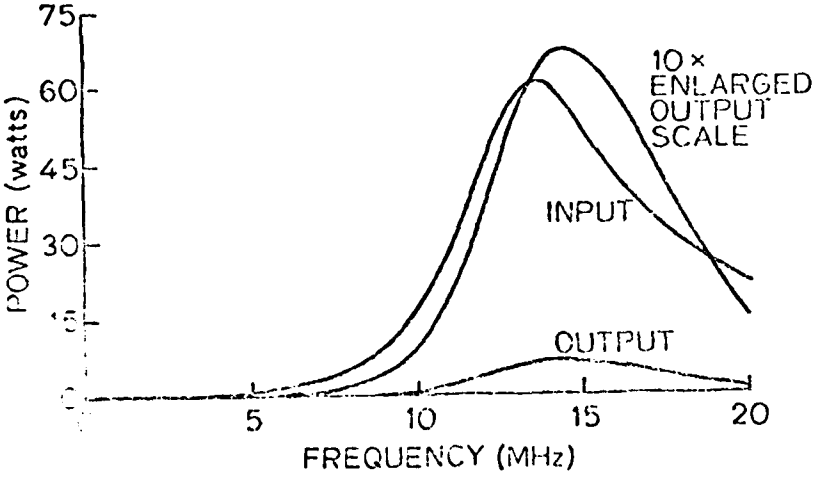

b. with tuning at resonance

FIG. 12 PVF_2 ELECTRICAL INPUT AND ACOUSTIC OUTPUT POWER FOR A 1A CURRENT DRIVE

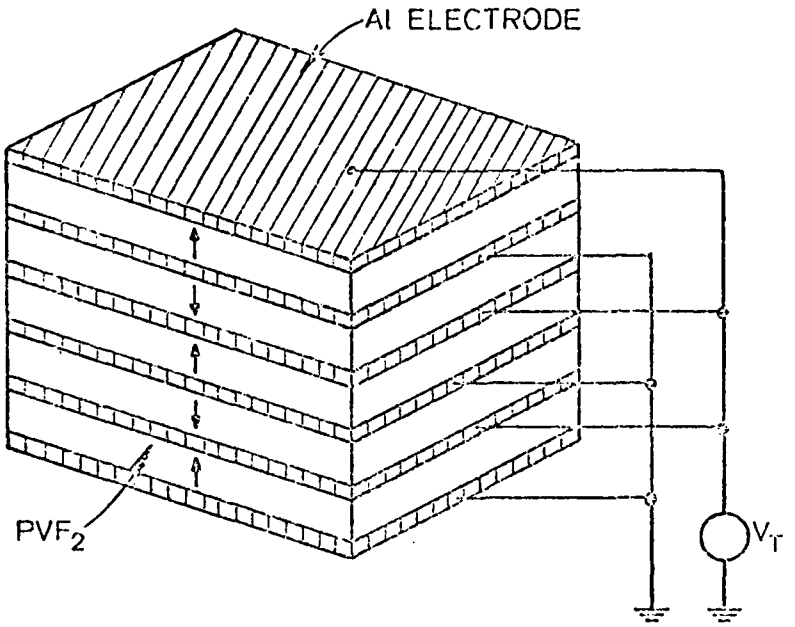

FIG. 13 MULTIPLE-LAYER TRANSMITTER

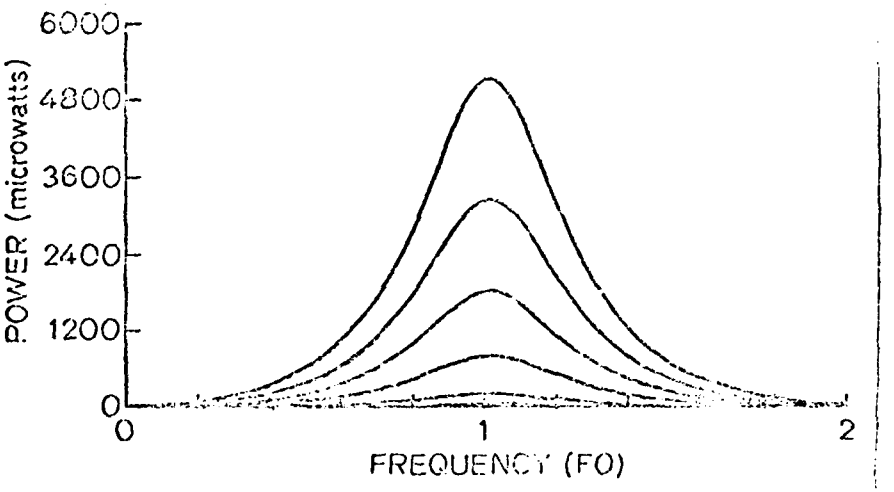

FIG. 14 NUMBER OF PVF_2 LAYERS VS OUTPUT POWER

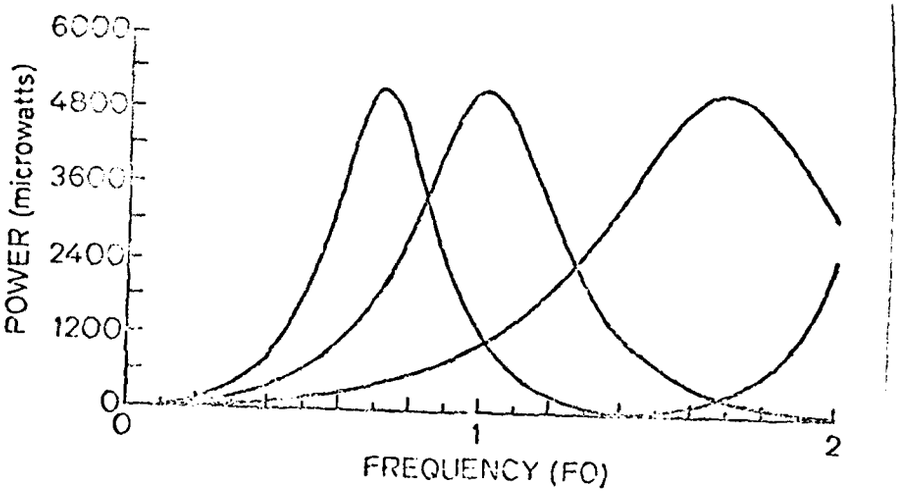

FIG. 15 NUMBER OF PVF_2 LAYERS VS RESONANT FREQUENCY

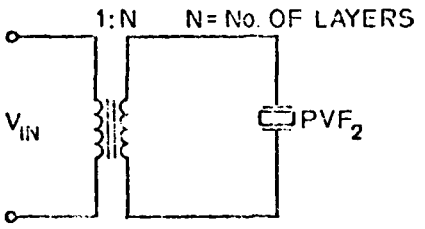

FIG. 16 ELECTRICAL MODEL OF A CONSTANT-THICKNESS PVF_2 TRANSDUCER COMPOSED OF LAYERS ELECTRICALLY IN PARALLEL.

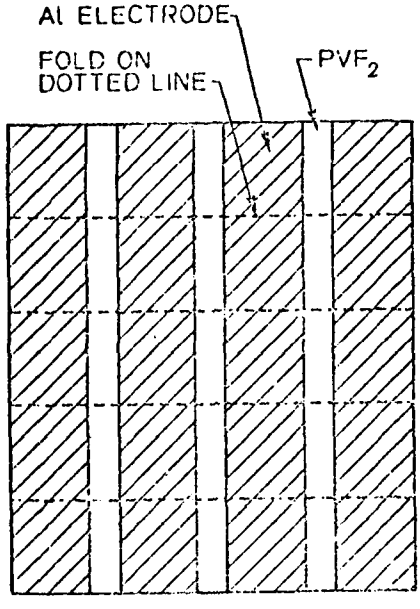

FIG. 17 MULTIPLE-LAYER PVF_2 FABRICATION SCHEME

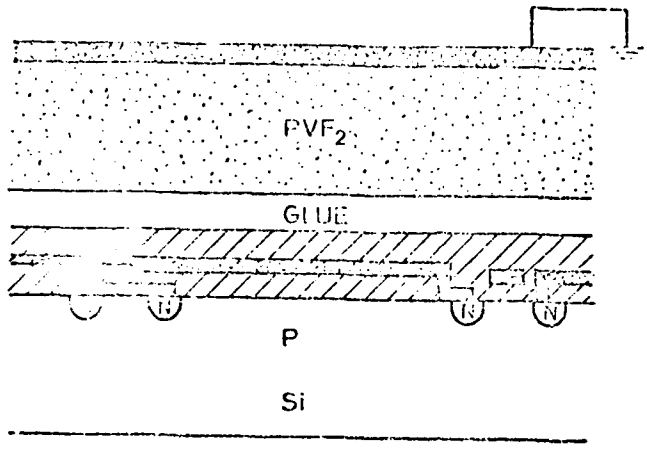

A. Cross section

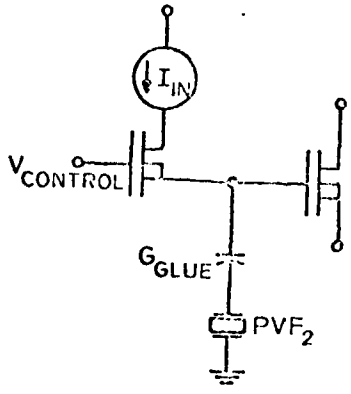

FIG. 18 TRANSMIT/RECEIVE INTEGRATED MONOLITHIC TRANSDUCER
B. Electrical equivalent circuit

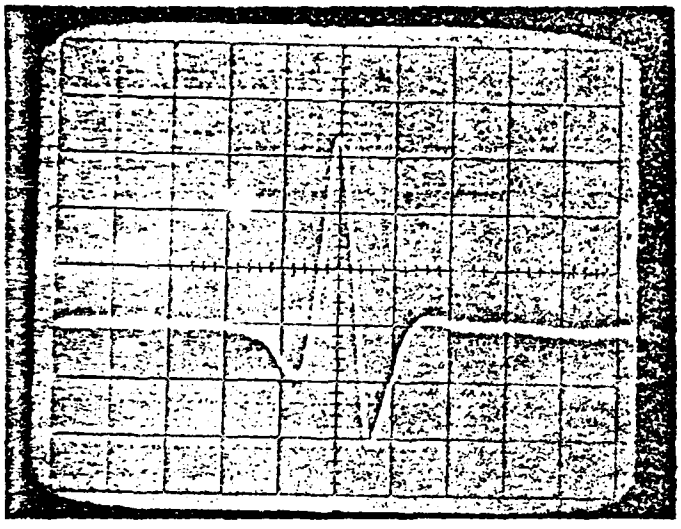

PVF_2 VOLTAGE DRIVE

→ 0.2 μsec/div

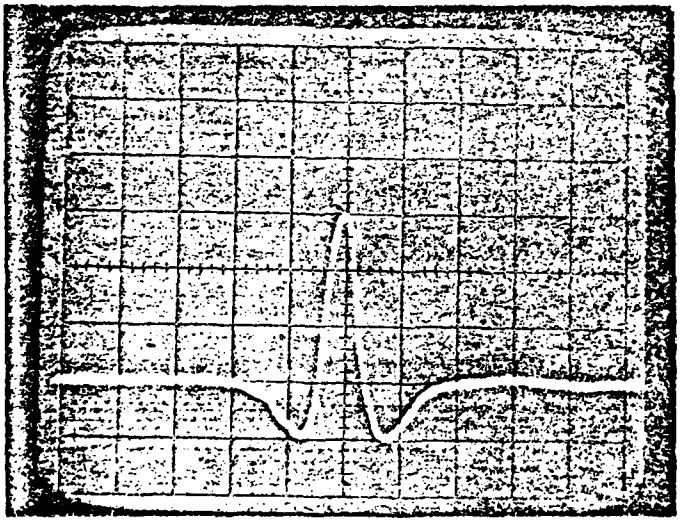

PVF_2 CURRENT DRIVE

FIG. 28 IMPULSE RESPONSE OF THE PVF_2 TRANSDUCER

a. Voltage drive
b. Current drive

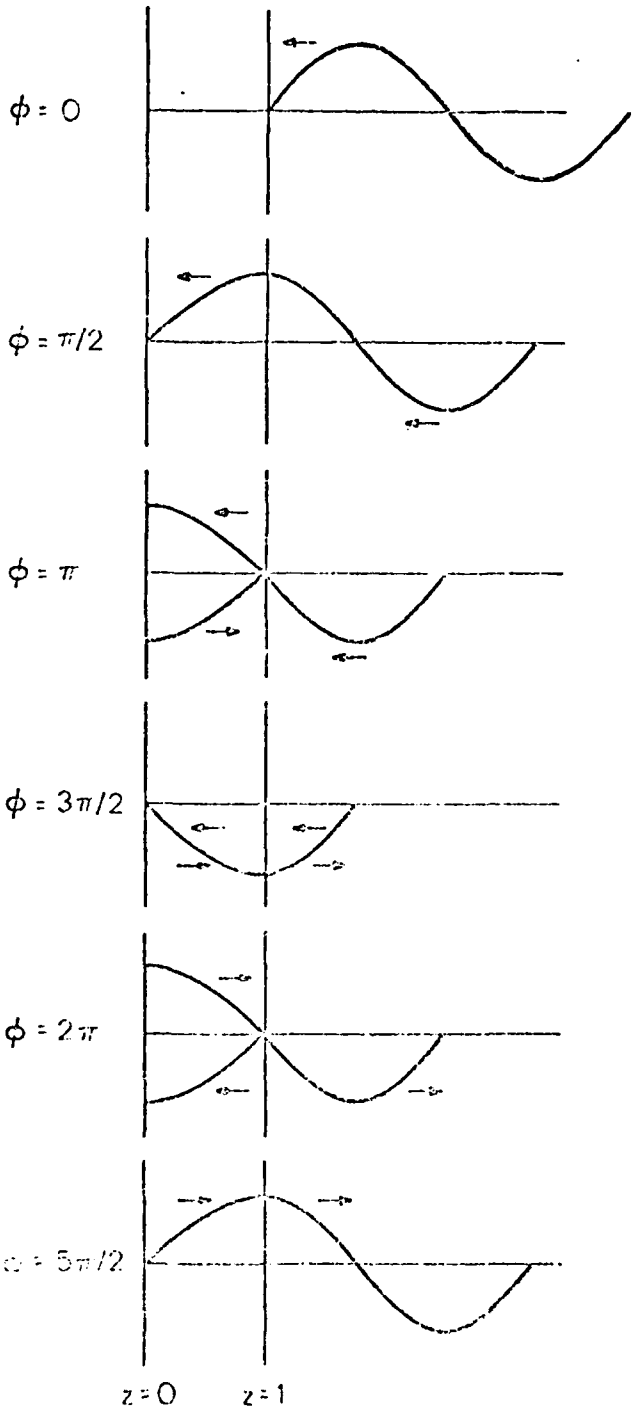

FIG. 20 DERIVATION OF IDEAL TWO-WAVE IMPULSE RESPONSE OF RIGIDLY BACKED PVF_2 TRANSDUCER

a. Progression with time of strain wave incident on PVF_2

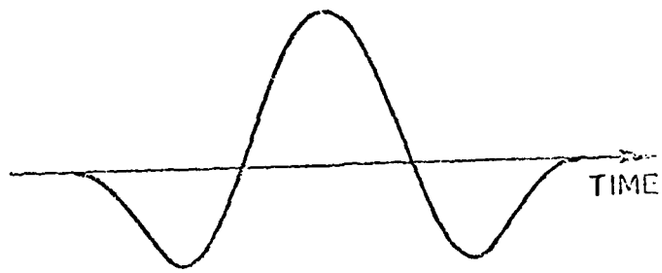

FIG.20 DERIVATION OF IDEAL TWO-WAVE IMPULSE RESPONSE OF RIGIDLY BACKED PLANE TRANSDUCER

a. Ideal two-way response

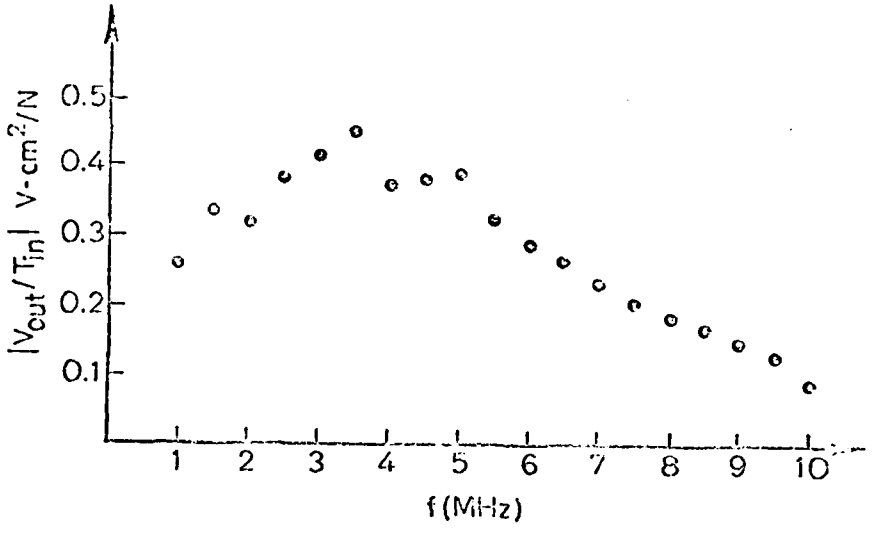

FIG. 21 MEASURED OUTPUT-VOLTAGE/INPUT-STRESS TRANSFER RELATIONSHIP VS FREQUENCY OF PVF_2 ARRAY ELEMENT

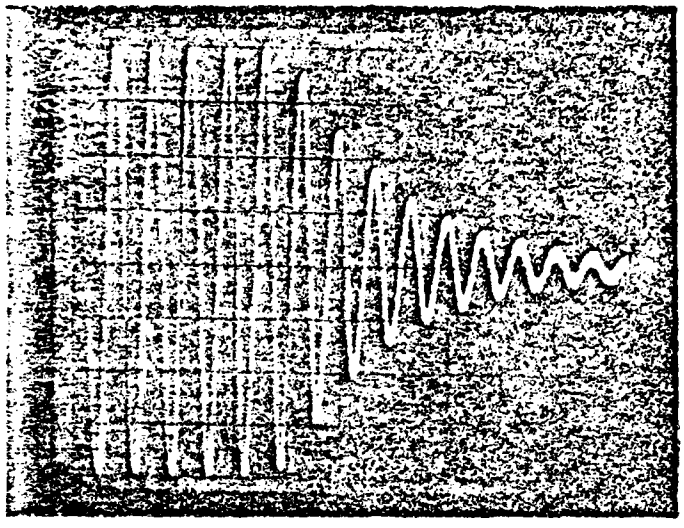

FIG. 22 STEP RESPONSE OF INDUCTOR-TUNED, CURRENT-SOURCE DRIVEN PVF_2 TRANSDUCER